UPPSALA
UNIVERSITET

Digital Comprehensive Summaries of Uppsala Dissertations from the Faculty of Pharmacy 280

Polymeric Nanoparticles as Carriers for Antimicrobial Peptides

Factors Affecting Peptide and Membrane Interactions

RANDI NORDSTRÖM

ACTA
UNIVERSITATIS
UPSALIENSIS
UPPSALA
2019

ISSN 1651-6192
ISBN 978-91-513-0778-7
urn:nbn:se:uu:diva-383639

Dissertation presented at Uppsala University to be publicly examined in Room A1:107a, BMC, Husargatan 3, Uppsala, Friday, 29 November 2019 at 09:15 for the degree of Doctor of Philosophy (Faculty of Pharmacy). The examination will be conducted in English. Faculty examiner: Professor Erica Wanless (School of Environmental and Life Sciences, University of Newcastle).

Abstract
Nordström, R. 2019. Polymeric Nanoparticles as Carriers for Antimicrobial Peptides. Factors Affecting Peptide and Membrane Interactions. *Digital Comprehensive Summaries of Uppsala Dissertations from the Faculty of Pharmacy* 280. 74 pp. Uppsala: Acta Universitatis Upsaliensis. ISBN 978-91-513-0778-7.

As resistance towards conventional antibiotics is becoming more pronounced, cationic antimicrobial peptides (AMPs) have received considerable attention as possible therapeutic alternatives. Thousands of potent AMPs occur in humans, animals, plants and fungi as a natural part of the immune system. However, there are several challenges with AMP therapeutics related to formulation and delivery. Examples include proteolytic sensitivity and serum protein binding, resulting in quick degradation, loss of activity and clearance. Therefore, it is important to find a suitable drug delivery system to meet these protection and delivery challenges. Micro-/nanogels are loosely crosslinked polymer colloids with high water content that can be made to trigger at a wide range of stimuli. They have shown promise as delivery systems for AMPs, as the aqueous environment they create allows the peptides to maintain their natural conformation, while their gel networks offer protection and triggered release. This thesis aims towards expanding the knowledge about degradable and non-degradable pH-responsive micro-/nanogels as carriers for AMPs.

The results in this thesis show that factors relating to the drug delivery system (degradability, charge and crosslinker density), the surrounding media (pH and ionic strength) and the peptide properties (length, charge, PEGylation) all affect the peptide loading to, protection, release from and effect of AMP-loaded gels. Studies of the interaction of AMP-loaded microgels with bacteria-modelling liposomes and lipid bilayers have verified peptide effect after gel incorporation, as further demonstrated by *in vitro* studies on several bacterial strains. Neutron reflectometry provided detailed mechanistic information on the interaction between AMP-loaded gels and bacteria-modelling lipid bilayers, showing that the antimicrobial unit is the released peptide. All gels showed low, promising hemolysis and some gels could offer protection against proteolytic degradation of AMPs.

In summary, non-degradable and degradable micro-/nanogels are versatile and interesting candidates as AMP carriers. Small changes in the gel composition or the AMP used can dramatically change the peptide loading, release and effect. It is therefore necessary to carefully consider and evaluate the optimal carrier for every AMP and the application at hand.

Keywords: antimicrobial peptide, microgel, degradable, nanogel, drug delivery, PEGylation, secondary structure, model membrane, lipid bilayer, neutron reflectometry, ellipsometry

Randi Nordström, Department of Pharmacy, Box 580, Uppsala University, SE-75123 Uppsala, Sweden.

ISSN 1651-6192
ISBN 978-91-513-0778-7
urn:nbn:se:uu:diva-383639 (http://urn.kb.se/resolve?urn=urn:nbn:se:uu:diva-383639)

"This isn't magic, is it?"
"I don't think so… It's probably just very very very strange science"
"Oh, good"… "Eh…What's the difference?"

\- *Terry Pratchett*

Family
[fæmily] noun
A group of people that I love.
They made this journey worth-while.

List of papers

This thesis is based on the following papers, which are referred to in the text by their Roman numerals.

I Nyström, L., **Nordström, R**., Bramhill, J., Saunders, B.R., Álvarez-Asencio, R., Rutland, M.W., Malmsten, M. (2016) Factors Affecting Peptide Interaction with Surface-Bound Microgels. *Biomacromolecules,* 17:669-678

II **Nordström, R**., Nyström, L., Andrén, O.C.J., Malkoch, M., Umerska, A., Davoudi, M., Schmidtchen, A., Malmsten, M. (2018) Membrane Interactions of Microgels as Carriers of Antimicrobial Peptides. *Journal of Colloid and Interface Science,* 513:141-150

III **Nordström, R**.*, Browning, K.L.*, Parra-Ortiz, E.*, Damgaard, L.S.E., Malekkhaiat-Häffner, S., Maestro, A., Campbell, R.A., Cooper, J.F.K. and Malmsten, M. Membrane Interactions of Antimicrobial Peptide-Loaded Microgels. *Submitted.*

IV **Nordström, R**.*, Nyström, L.*, Ilyas, H., Atreya, H.S., Borro, B.C., Bhunia, A., Malmsten, M. (2019) Microgels as Carriers of Antimicrobial Peptides – Effects of Peptide PEGylation. *Colloids and Surfaces A: Physiochemical and Engineering Aspects,* 565:8-15

V **Nordström, R**., Andrén, O.C.J., Singh, S., Malkoch, M., Davoudi, M., Schmidtchen, A., Malmsten, M. (2019) Degradable Dendritic Nanogels as Carriers for Antimicrobial Peptides. *Journal of Colloid and Interface Science,* 554:592-602

Reprints were made with permission from the respective publishers.
** These authors contributed equally.*
I was highly involved in the planning, study design, experimental work, data analysis and writing of Papers II, III and V and partly involved in Papers I and IV. I did not contribute to any larger extent to the experimental work concerning the *in vitro* data included in the papers above.

Additional papers not included in this thesis.

VI Braun, K., Pochert, A., Lindén, M., Davoudi, M., Schmidtchen, A., **Nordström, R**., Malmsten, M. (2016) Membrane Interactions of Mesoporous Silica Nanoparticles as Carriers of Antimicrobial Peptides. *Journal of Colloid and Interface Science,* 475:161-170

VII **Nordström, R**., Malmsten, M. (2017) Delivery Systems for Antimicrobial Peptides. *Advances in Colloid and Interface Science,* 242:17-34

VIII Malekkhaiat Häffner, S., Nyström, L., **Nordström, R**., Xu, Z.P., Davoudi, M., Schmidtchen, A., Malmsten, M. (2017) Membrane Interaction and Antimicrobial Effects of Layered Double Hydroxide Nanoparticles. *Physical Chemistry Chemical Physics,* 19(35):23832-23842

IX Parra-Ortiz, E., Browning, K.L., Damgaard, L.S.E., **Nordström, R**., Micciulla, S., Bucciarelli, S., Malmsten, M. (2019) Effects of Oxidation on the Physiochemical Properties of Polyunsaturated Lipid Membranes. *Journal of Colloid and Interface Science,* 538:404-419

X Boge, L., Browning, K.L., **Nordström, R**., Campana, M., Damgaard, L.S.E., Seth Caous, J., Hellsing, M.S., Ringstad, L., Andersson, M. (2019) Peptide-Loaded Cubosomes Functioning as an Antimicrobial Unit Against Escherichia coli. *ACS Applied Materials and Interfaces,* 11(24): 21314-21322

XI Zhang, Y., Andrén, O. C. J., **Nordström, R**., Fan, Y., Malmsten, M., Mongkhontreerat, S., Malkoch, M. (2019) Off-Stoichiometric Thiol-Ene Chemistry to Dendritic Nanogel Therapeutics. *Advanced Functional Materials*, 1806693

Patent application, not included in this thesis.

XII Polymer Factory Sweden AB, Andrén, O. C. J., Malkoch, M., Zhang, Y., **Nordström, R**., (2018) Dendritic Nanogel Carriers and Method of Production. No. 1850975-2

Contents

Abbreviations

AFM	Atomic force microscopy
AMP	Antimicrobial peptide
ATCC	American type culture collection
ATR	Attenuated total reflectance
b	Neutron scattering length
BCA	Bicinchoninic acid
BDD	1,4-Butanediol diacrylate
CCD	Charge-coupled device
CD	Circular dichroism
CF	Carboxyfluorescein
CFU	Colony-forming units
Chol	Cholesterol
CL	Cardiolipin
Cryo-TEM	Cryogenic transmission electron microscopy
DLD	Dendritic-linear-dendritic
DLS	Dynamic light scattering
DMPC	1,2-Dimyristoyl-sn-glycero-3-phosphocholine
DMPG	1,2-Dimyristoyl-sn-glycero-3-phosphorylglycerol sodium salt
DNA	Deoxyribonucleic acid
DNG	Dendritic nanogels
DOPC	1,2-Dioleoyl-sn-glycero-3-phosphocholine
DOPE	1,2-Dioleoyl-sn-glycero-3-phosphoethanolamine
DOPG	1,2-Dioleoyl-sn-glycero-3-phospho-(1'-rac-glycerol) sodium salt
E. coli	*Escherichia coli*
EA	Ethyl acrylate
FTIR	Fourier transform infrared spectroscopy
GOPS	3-glycidoxypropyltrimethoxysilane
LDH	Layered double hydroxide
LPS	Lipopolysaccaride
MAA	Methacrylic acid
MAA microgels	Poly (methacrylic acid/butane diol diacrylate/ethyl acrylate) microgels
MIC	Minimal inhibitory concentration
MRSA	Methicillin resistant *Staphylococcus aureus*

NMR	Nuclear magnetic resonance
NOE	Nuclear Overhauser effect
NOESY	Nuclear Overhauser effect spectroscopy
NR	Neutron reflectometry
NTA	Nanosight tracking analysis
PC	Phosphatidylcholine
PCS	Photon correlation spectroscopy
PEG	Poly(ethylene glycol)
PG	Phosphatidylglycerol
PI	Phosphatidylinositol
P-Lys	Poly-L-lysine
PS	Phosphatidylserine
PSA	*Pseudomonas aeruginosa*
QCM-d	Quartz crystal microbalance with dissipation monitoring
QNM	Quantitative nanomechanical property mapping
RCSB PDB	Research collaboratory for structural bioinformatics protein data bank
RDA	Radial diffusion analysis
S. aureus	*Staphylococcus aureus*
SDS	Sodium dodecyl sulfate
SEM	Scanning electron microscopy
SLD	Scattering length density
STD	Saturation transfer difference
TOCSY	Total correlated spectroscopy
Tris	Tris (10mM, pH 7.4) buffer
Tris-NaCl	Tris (10mM, pH 7.4, 150 mM NaCl) buffer
VCA	Viable count analysis

Amino acids

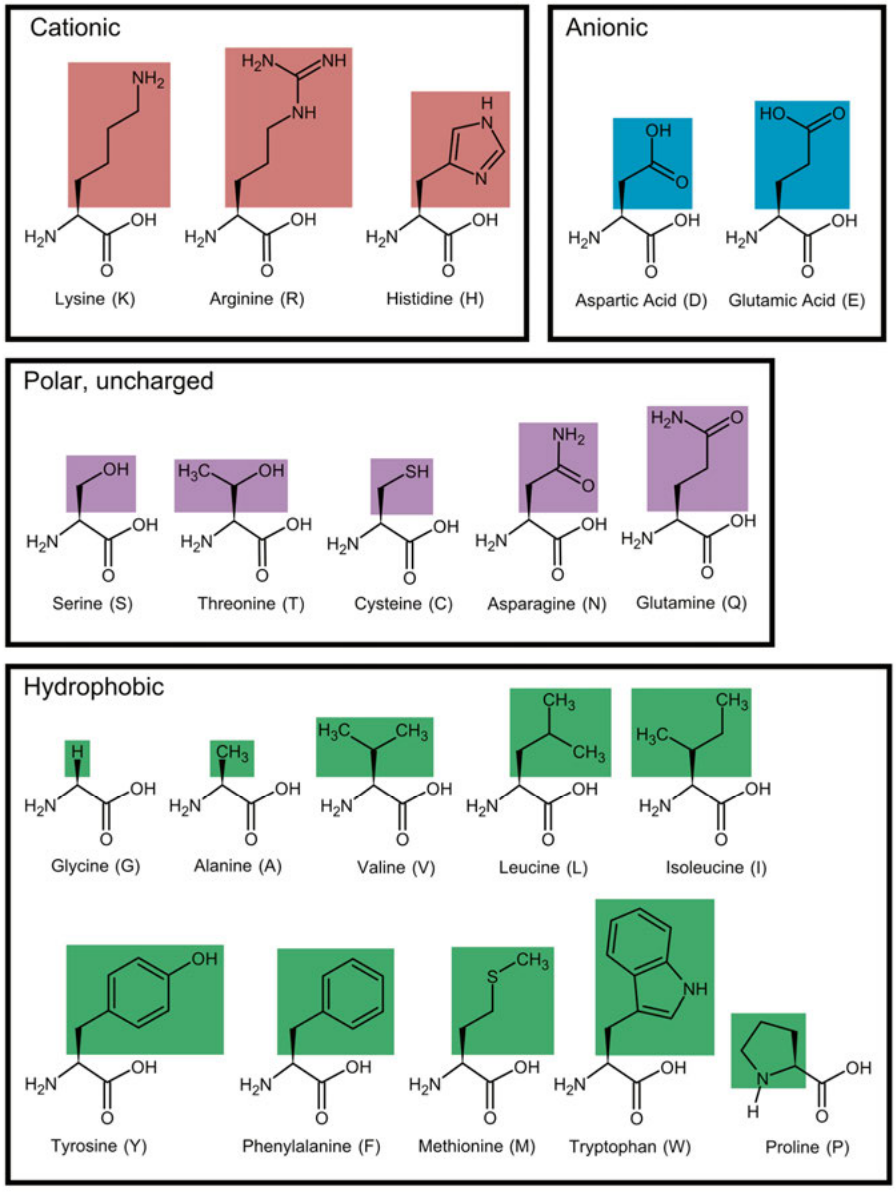
Cationic
Lysine (K)
Arginine (R)
Histidine (H)
Anionic
Aspartic Acid (D)
Glutamic Acid (E)
Polar, uncharged
Serine (S)
Threonine (T)
Cysteine (C)
Asparagine (N)
Glutamine (Q)
Hydrophobic
Glycine (G)
Alanine (A)
Valine (V)
Leucine (L)
Isoleucine (I)
Tyrosine (Y)
Phenylalanine (F)
Methionine (M)
Tryptophan (W)
Proline (P)

Lipids and cholesterol

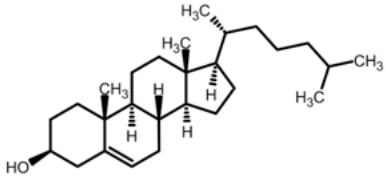

Cholesterol

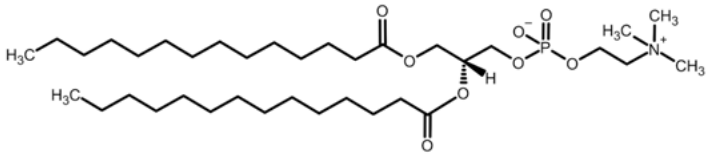

DMPC - 1,2-dimyristoyl-sn-glycero-3-phosphocholine

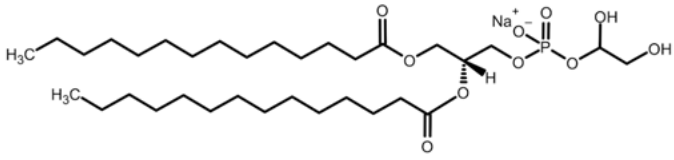

DMPG - 1,2-dimyristoyl-sn-glycero-3-phosphorylglycerol sodium salt

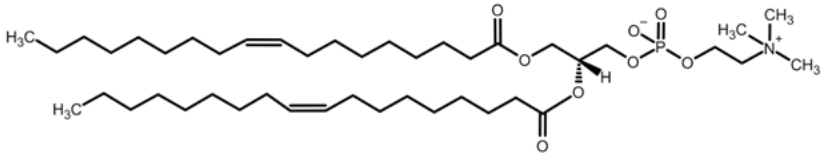

DOPC - 1,2-dioleoyl-sn-glycero-3-phosphocholine

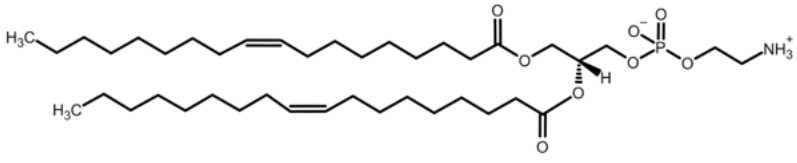

DOPE - 1,2-dioleoyl-sn-glycero-3-phosphoethanolamine

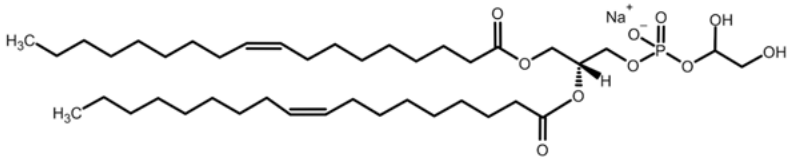

DOPG - 1,2-dioleoyl-sn-glycero-3-phospho-(1'-rac-glycerol) sodium salt

1. Introduction

Resistance development against commonly used antibiotics is ever increasing. Today. it is considered to be one of the major threats to world health and development according to the World Health Organization.[1] The United States Food and Drug Administration have listed 21 pathogens as serious threats to public health based on their resistance to antibiotics.[2] The European Union has systematically monitored resistant bacterial strains for many years. The number of infections due to just 10 of the monitored resistant strains has increased from 240,000 in 2007 to 600,000 in 2015. Mortality rose from 11,000 to 27,000 within the same timeframe.[3,4] The Public Health Agency of Sweden reported a projection where the number of Swedish patients suffering from four resistant strains was expected to increase from 15,000 cases in 2016 to 70,000 cases in 2050, with an accumulated social cost of 15.8 billion Swedish kronor (~1.5 billion euro).[5] We have only ourselves to blame, due to our overuse of antibiotics and poor follow-through of treatments. Antibiotics are also overused in a wide range of commercial areas, from cattle feed to detergents, resulting in an ever increasing number of resistant bacterial strains. Regardless of the cause of widespread antimicrobial resistance, alternative methods for dealing with severe bacterial infections are needed if we want to continue to treat these diseases with the ease we have since Alexander Fleming discovered the bactericidal effect of penicillin.[6]

Many different alternatives to antibiotics have been suggested by researchers for treatment of resistant strains, including antibodies,[7] vaccines,[8] antimicrobial peptides[9] and bacteriophages.[10,11] This thesis is a contribution to the research field exploring antimicrobial peptides as possible therapeutic alternatives. In particular, the thesis is focused on the formulation and delivery of fragile large peptides.

1.1 Antimicrobial peptides

Antimicrobial peptides (AMPs) are a class of molecules that have received considerable attention as possible alternatives to traditional antibiotics. AMPs are amphiphilic molecules, 10–15 amino acids long, commonly bearing a net positive charge.[12] Most AMPs are of natural origin, being part of the innate immune system of humans, animals, plants or fungi. Other AMPs are entirely

synthetic and have been developed for desired activities.[9,13] Bacteria have co-existed and co-evolved with AMPs without developing significant resistance.[14] Antimicrobial peptides attack bacteria through several routes including inhibition of enzymatic activity or cell wall, DNA, or protein synthesis. However, their main mode of action is through disruption of the bacterial cell wall. The interaction is largely electrostatic, occurring between the cationic AMPs and anionic bacterial membranes.[15] The mechanism of this membrane interaction differs depending on bacterial strain, AMP, and concentration. Commonly proposed mechanisms are (i) the carpet model (AMP adsorption parallel to the bilayer until critical coverage is reached and membrane disruption follows, in a detergent-like manner), (ii) the toroidal pore model (perpendicular AMP insertion, inducing a membrane curvature and pore formation lysing the membrane), and (iii) the barrel-stave model (also perpendicular peptide insertion and pore formation, but without the membrane curvature in (ii)). A schematic description of the common mechanisms of bacterial disruption by AMPs is shown in *Figure 1*.[16–18]

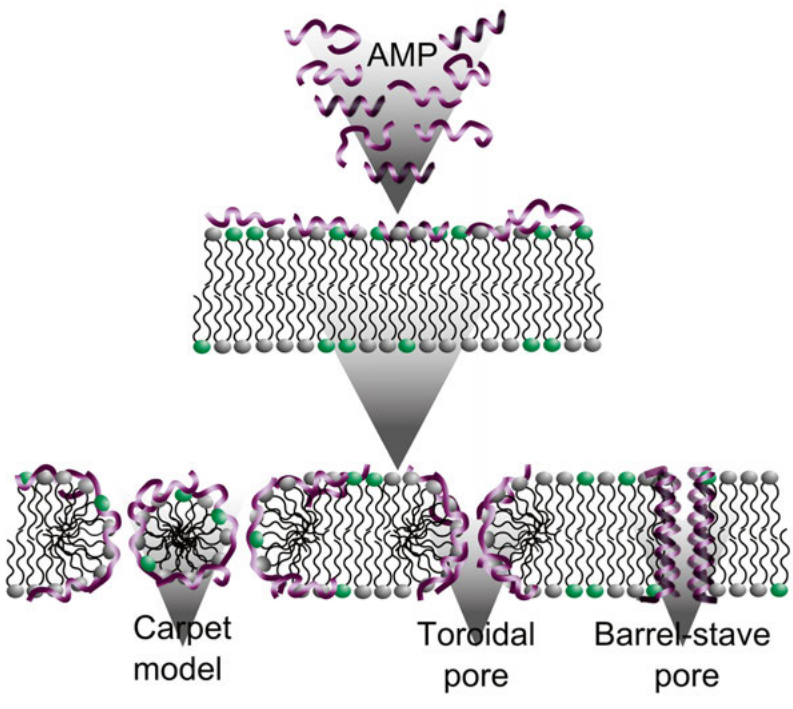

Figure 1. Schematic illustration of three proposed modes of action for antimicrobial peptides to lyse bacterial membranes: The carpet model (left), with AMP adsorption parallel to the membrane and a detergent-like membrane lysis. The toroidal pore model (centre), with perpendicular AMP insertion inducing membrane curvature and pore formation lysing the membrane. The barrel-stave model (right), with perpendicular peptide insertion, but without membrane curvature.[16–18]

Although development of natural resistance to AMPs *in vivo* is low, an increased resistance to AMPs has been observed in research projects and product development.[15,19,20] Four important modes of resistance against AMPs are (i) increased proteolytic activity, degrading AMPs, (ii) increased active efflux of AMPs, (iii) membrane modifications leading either to decreased anionic charge reducing the electrostatic attraction of AMPs or to protein-lipid patches and (iv) external trapping and inactivation of AMPs through production of anionic species.[15,21,22] Compared with traditional antibiotics, the expression of these resistance mechanisms commonly decreases the fitness of bacteria in terms of growth rate, starvation survival and growth, in mice.[15] Due to resistance development, AMPs will not be the final answer to the problem of infectious disease; they are only one weapon in our toolbox to continue fighting bacterial infections. As bacteria evolve, our methods of treating infections must also evolve. By learning from our mistakes with penicillin and through careful and clever usage of AMPs, we may be able to delay or partially prevent future resistance development.

1.1.1 Selected peptides

The peptides used in this thesis were selected on the basis of several factors. These are mainly related to the structure and function of the peptides, but also their availability. Structural properties include peptide length, charge, secondary structure and post-translational modifications. Functional aspects include proteolytic stability, toxicity and immunomodulation. The selected peptides are presented in *Figure 2* and *Table 1* and are described in detail below.

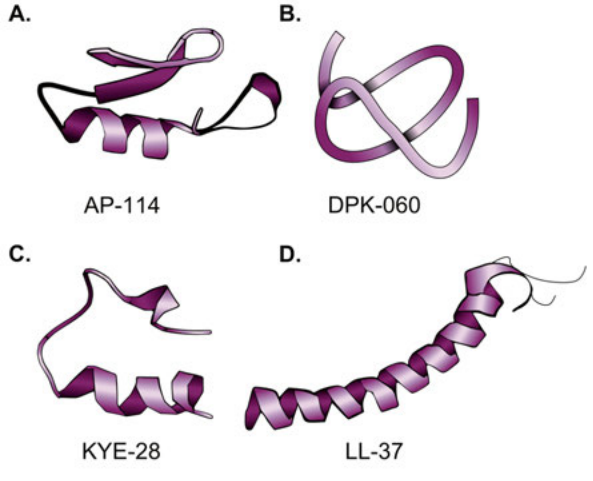

Figure 2. Illustrations of the secondary structures of the peptides used in this thesis: (A) AP-114[23], containing both α-helix and β-sheet conformations, (B) DPK-060 in random coil, (C) KYE-28[24] in α-helix conformation at the C-terminal, and (D) LL-37[25] with its pronounced α-helix. Illustrations A, C and D are adapted from RCSB Protein Data Bank.[26] Their amino acid sequences can be found in *Table 1*.

Table 1. Selected properties of peptides used in this thesis and references to papers where they are included.

Model peptides					
	Sequence	*Mw*[a]	*Z*[b]	*H*[c]	*Paper*
Poly-L-lysine	$(KKK)_n$	4,200	+32	-3.9	I
		10,500	+81	-3.9	I
		149,000	+1,153	-3.9	I
Antimicrobial peptides					
AP-114	GFGCNGPWNEDDLRCHN HCKSIKGYKG-GYCAKGGFVCKCY	4,274	+3	-0.7	II
DPK-060	GKHKNKGKKNGKH-NGWKWWW	2,505	+7	-2.5	II, V
KYE-28	KYEITTI-HNLFRKLTHRLFRRN-FGYTLR	3,595	+6	0.7	IV
KYE-28PEG	KYEITTI-HNLFRKLTHRLFRRN-FGYTLR-PEG48	5,851	+6		IV
PEG**KYE-28**PEG	PEG24-KYEITTI-HNLFRKLTHRLFRRN-FGYTLR-PEG24				IV
PEG**KYE-28**	PEG48-KYEITTI-HNLFRKLTHRLFRRN-FGYTLR				IV
LL-37	LLGDFFRK-SKEKIGKEFKRIVQRI-FLRNLVPRTES	4,364	+6	-0.6	II, III, V

a) Mw: Molecular weight (g/mol).
b) Z_{net}: Net charge at pH 7.4
c) H: Mean hydrophobicity on the Kyte-Doolittle scale.[27]

Poly-L-Lysine (P-Lys) is not an active AMP, rather it is a well-used model for AMPs when evaluating carrier systems.[28] In this thesis, it was used as a model to map interactions between cationic peptides and anionic drug carrier systems. The different peptide lengths were utilised to monitor the effects of electrostatic interactions and peptide molecular weight, but also to study mesh size limitations of the polymer network of the carrier, which will be further discussed later.[28]

AP-114 (also reported as NZ-2114 in literature) is a peptide found in the *Pseudoplectania nigrella* fungus. The peptide has a segment with β-sheet conformation and another with α-helix conformation, see *Figure 2A*.[29,30] Its mechanism of action is a toroidal-pore mechanism and it targets the cellular precursor Lipid II, thereby inhibiting membrane biosynthesis.[31] AP-114 is active

against Gram-positive bacteria, also against resistant strains such as methicillin-resistant *Staphylococcus aureus* (*MRSA*), making it a good candidate for treatment of pneumonia.[32]

DPK-060 (also reported as GKH17-WWW in literature) is a synthetically modified peptide with origin in the human protein kininogen.[33,34] The peptide is proteolytically stable and has shown a broad-spectrum antibacterial effect. DPK-060 does not have a defined secondary structure, see *Figure 2B*. The AMP has a tryptophan tag at its C-terminal, which has been shown to increase selectivity of bacterial membranes over mammalian ones, as well as to increase the antimicrobial effect on clinical isolates and resistant strains.[33,35] The intended application for the peptide is topical delivery, and it has shown promising results in phase II studies of infections in atopic dermatitis.[36]

KYE-28 is a multifunctional peptide being both broad-spectrum antimicrobial,[37,38] antifungal,[39] and immunomodulating through down-regulation of the proteolytic activity in infected tissue.[40] The peptide is derived from human heparin co-factor II and consists of the D-helix of the protein, see *Figure 2C*.[40] The immunomodulatory effect makes it a suitable candidate for drug delivery at implant sites.[41] In this thesis, we also study PEGylated (covalently attached polyethylene glycol units) variants of KYE-28. PEGylations of peptides have a number of favourable effects, including decreased binding to serum proteins,[42] increased circulation times[43] and increased stability towards proteases.[44] In addition, it has been shown that PEGylation of KYE-28 decreases toxicity of the peptide in a M_w(PEG)-dependent manner, whereas anti-inflammatory effects remain largely unaffected by PEGylation.[38]

LL-37 is a well-studied linear AMP of human origin with a broad-spectrum effect on bacteria and potent antiviral and immunostimulatory effects.[45,46] It is part of the innate immune system in the skin and soft tissue and has proven to be a potent candidate for chronical wound healing.[47] Depending on the saturation of lipid tails, the mechanism of membrane interaction of LL-37 has been proposed to be either a carpet or toroidal pore model.[48,49] Depending on the conditions, LL-37 will adopt either a random coil or a helical structure. Helix formation is most pronounced when binding to a membrane or loaded into anionic carrier systems, see *Figure 2D*.[50,51] LL-37 is both sensitive to proteolytic degradation and toxic to human cells in high concentrations and therefore requires a carrier system that can protect the peptide and reduce toxicity.[52]

Although AMPs have shown broad-spectrum antimicrobial effects, also against resistant strains, there are a number of challenges which must be overcome for these peptides to reach the pharmaceutical market to any greater extent. Firstly, if the AMP is administered parenterally, the positively charged

peptides can bind to negatively charged serum proteins resulting in fast clearance or accumulation in the mononuclear phagocytic system, risking toxicity and reduced systemic effect.[38,44,53,54] Secondly, some infections, for example tuberculosis, act intracellularly, making AMP delivery without killing the host macrophages challenging.[55–57] Finally, AMPs are usually sensitive to the high proteolytic activity in infected tissue, caused by bacterial and human proteases, resulting in AMP degradation.[52,58]

To meet these challenges, different drug carrier systems have been suggested for the delivery of AMPs.[59–61] However, in contrast to the extensive efforts spent on the discovery and development of potent AMPs, drug carrier and delivery aspects have been much less investigated.[59] This is despite the fact that efficient drug delivery vehicles can provide positive effects such as prolonged AMP circulation and synergistic effects,[62,63] increased mycobacterial killing,[64] protection against proteolysis,[50] increased stability,[65] reduced toxicity,[50] and triggered peptide release.[66]

1.2 Drug delivery systems for AMPs

A wide range of drug delivery systems have been suggested for antimicrobial peptides to protect the peptides from chemical and enzymatic attacks and to facilitate delivery, as described in Section 1.1.[59] In addition to the challenges already mentioned, the therapeutic onset of most AMPs is in the μM range. As AMPs are either synthesised by sequence or produced by cells/bacteria, methods which are expensive to scale up for production, cost-of-goods is a key issue for development of AMPs into therapeutics.[67] Therefore, many applications aim to use drug delivery systems to achieve a local delivery or a locally raised AMP concentration, decreasing the amount of required peptide dramatically as compared to systemic delivery of peptides.

Suggested delivery systems include, but are not limited to, inorganic delivery systems (e.g., mesoporous silica,[68–70] metal nanoparticles[71,72] and graphene oxide[73,74]), dispersions and self-assembly systems (e.g., cubosomes[75] and liposomes[76,77]), and polymer materials (e.g., fibres,[78] multilayers[79,80] and gels[81,82]), with the latter being the focus of this thesis.

1.2.1 Polymeric delivery systems

Polymer materials are frequently used as drug delivery systems, since the endless toolbox of organic chemistry enables fine-tuning of polymer functionality to suit the application at hand. In the context of peptide delivery, polymeric materials have been used to tune peptide loading,[81,83] prolong release rates,[84]

protect peptides from proteolytic degradation,[50] minimise bacterial adhesion,[85] and increase antimicrobial activity.[86]

Exemplifying this, encapsulation of the AMP nisin into self-assembled nanoparticles of poly-γ-glutamic acid and chitosan has shown that the presence of chitosan improves the colloidal stability through increased zeta potential, increases nisin encapsulation efficiency, and prolongs nisin release time, see *Figure 3*.[84] In addition, the nisin-loaded poly-γ-glutamic acid/chitosan composite particles inhibits *Escherichia coli* (*E. coli*) growth more efficiently than either nisin alone or nisin-loaded poly-γ-glutamic acid particles.[84]

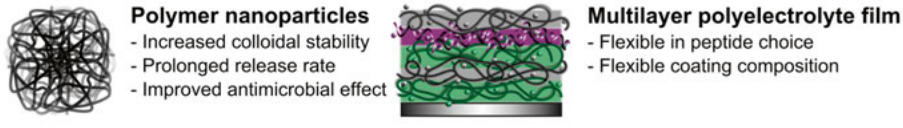

Figure 3. Example of two polymer-based carrier systems for AMPs, nanoparticles of poly-γ-glutamic acid and chitosan and a multilayer polyelectrolyte film, and their main advantages.[84,85]

Another example is a multilayer polyelectrolyte film used as an implant coating. The film consists of polyethylene amine, poly(sodium 4-styrenesulfonate), poly-allylamine-hydrochloride, poly-L-glutamic acid, and poly-L-lysine, and carries a defensin.[87] The coating is deposited layer-by-layer, see *Figure 3*, enabling flexibility in the choice of AMPs used, as well as providing an opportunity to use several different peptides on the same surface, increasing efficiency and minimising the risk of bacteria surviving due to resistance.

1.2.2 Polymeric gels as AMP delivery systems

Polymer (micro)gels are a special case of polymeric nanoparticle delivery systems, and the main focus of this thesis. Microgels are loosely cross-linked polymer colloids, commonly with a high water content. The aqueous environment enables peptides and proteins to maintain a natural conformation within the gel, minimising the risk of premature degradation and inactivation. Therefore, polymer gels have received considerable attention as delivery systems for peptides and proteins.[88,89] Polymeric gels can show dramatic swelling reactions to a range of stimuli, such as pH,[90,91] temperature,[92–94] redox conditions[95,96] or certain metabolites,[97,98] but also in response to externally applied forces such as magnetic fields[99,100] and light,[101] enabling triggered release of peptides and drugs.

Beneficial properties of AMP-loaded gels include high peptide loading,[102] triggered release,[102] reduced peptide toxicity,[81] proteolytic stabilisation[103] and improved antimicrobial effect.[82] A variety of gels have been combined with

AMPs to achieve antimicrobial effects, including hyaluronic acid micro- and nanogels,[81,82] chitosan microgels,[104] ε-methacrylamide hydrogels[105] and PEG-based hydrogels.[106] For example, self-assembled hyaluronic acid nanogels (see *Figure 4*), loaded with the LL-37 analogue LLKKK18, were used to treat tuberculosis.[82] It was shown that incorporation of LLKKK18 in the nanogels allowed considerable peptide loading until neutralisation of the hyaluronic acid was achieved. The gels protected the peptide from proteolytic degradation. The peptide-loaded nanogels also showed improved uptake by tuberculosis-infected macrophages, leading to a decreased mycobacterial load.[82]

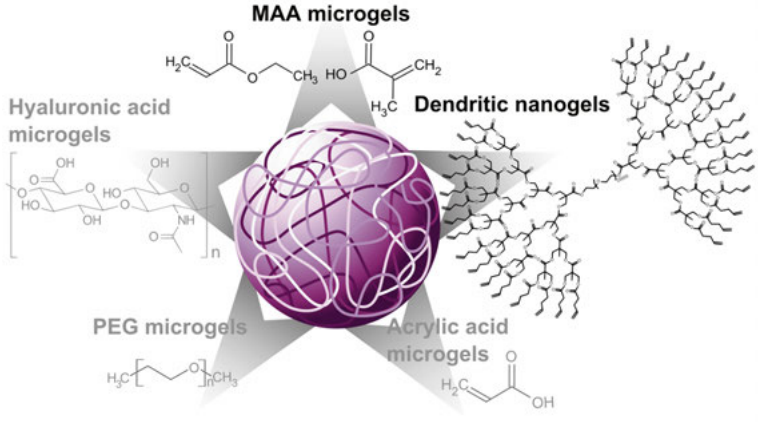

Figure 4. Schematic of a few examples of nano- and microgels suggested as AMP carriers, literature examples in grey and the systems used in this thesis in black. Both model peptide and AMP interactions with methacrylic acid-based microgels (MAA microgels) have been reported.[50,102] Degradable dendritic nanogels (DNGs) have been suggested as carriers for both doxorubicin and the AMPs LL-37 and DPK-060.[107,108] Peptide interactions with acrylic acid microgels have been extensively studied.[109,110] Cross-linked PEG hydrogel coatings with the AMP CysHHC10 have been suggested as biomaterials coatings.[103,106] Hyaluronic acid microgels and nanogels have been used as carriers for the AMPs Novicidin and LLKKK18.[81,82]

In another example, an antimicrobial coating was formed from an alkene-functionalised PEG, a thiol cross-linker and the AMP CysHHC10 (CKRWWKWIRW). Through single step thiol-ene chemistry, the components formed a thin hydrogel which could be used as a biomaterial coating, see *Figure 4*.[103] The covalent incorporation of peptide in the gel increased its stability in human serum over time.[103] In addition, the coating displayed potent antimicrobial effects against biofilm-forming *S. aureus* and *S. epidermidis*.[106]

Previously, the interactions of model peptides with pH-responsive acrylic acid-based microgels with a diameter of around 100 µm have been studied, see *Figure 4*.[109,110] The effect of peptide length,[102,111,112] type of charged group of the peptide[113] and charge distribution,[109] hydrophobicity distribution,[114] and

secondary structure[115], as well as gel charge density[110,116] and mesh size limitations[111], were investigated. pH and ionic strength of the surrounding media have been shown to affect peptide loading, release, and the antimicrobial effect, due to electrostatic interactions and screening.[28,117,118] Despite such previous studies, it is challenging to predict how differently charged amphiphilic molecules such as AMPs will behave in a microgel system; small changes to charge, hydrophobicity distribution and length can dramatically affect the interactions. All of these factors have to be carefully considered in order to draw relevant conclusions regarding microgels as AMP carrier systems.

Reducing gel size decreases the risk of peptide scavenging. This is due to a larger surface area per volume ratio leading to smaller diffusion distances within the gels, facilitating peptide release.[12,67,119] Reducing gel size can also bring advantages, such as increased bioavailability and circulation times.[120] This, in combination with peptide protection and triggered release, as mentioned above, makes micro-/nanogels interesting as AMP carrier systems. Two previously reported gel types, both on the order of 100 nm in diameter,[90,108] are used in the present work. For consistency, the terminology used here is coordinated with earlier literature, resulting in one microgel library and one nanogel library, despite them having the same size range.

The two gel libraries investigated in this thesis as AMP carrier systems are methacrylic acid-based microgels (MAA microgels) and degradable dendritic nanogels (DNGs), *Figure 4*.[28,50] The synthesis of the MAA microgels is described in Section 3.1. The DNG library is described in Section 1.2.3, while the synthesis thereof is not included in this thesis work. Both gel libraries are functionalised with carboxylic acids, leading to anionically charged AMP-binding sites at physiological pH. These anionic moieties can be triggered to release peptides through a pH change or by increasing the ionic strength.[50] Both the MAA microgel library and the DNG library are versatile in composition, hence both the charge and cross-linker densities can be tuned in the synthesis, without affecting the size and polydispersity index of the particles.[121,122] The varying charge density of these systems enables us to investigate the importance of charge contrast between microgel and AMP.

1.2.3 Degradable nanogels

For many applications, the main advantage of a degradable drug delivery system is the possibility to control release rate through network degradation.[123] For antimicrobial applications, however, a fast release with a high resulting peptide concentration is usually preferred to ensure peptide release well above the threshold for bacterial killing, hence minimising resistance development.[124–126] Here, the advantage of degradability is instead that accumulation,

long-term toxicity or removal of the drug delivery system need not be considered.[127] Well-studied and biocompatible building blocks and degradation products contribute to a safer drug delivery system.[128] The nanogel library used here is versatile and degradable over a reasonable time period (~10 days). The systems are composed of cross-linked dendritic-linear-dendritic (DLD) structures. The suggested network architecture of the DNGs is unconventional, schematically presented in *Figures 4* and *5*.

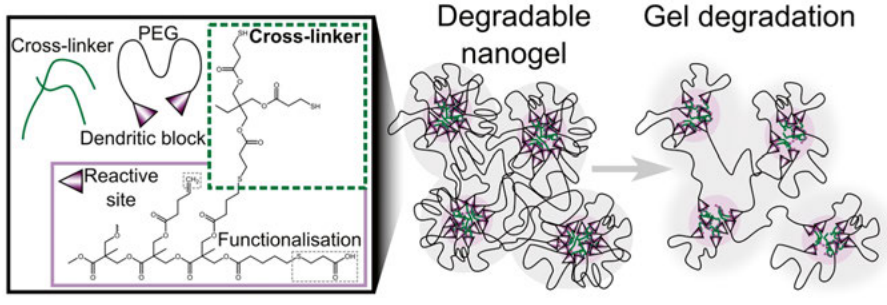

Figure 5. (Left) Chemical structure of the hyperbranched part of the DLD structure. (Centre) Schematic illustration of the DNG structure with several charged and cross-linked cores covered with a PEG corona. (Right) Schematic illustration of a partially degraded DNG structure.

The linear part consists of a PEG moiety and the dendritic part is a hyperbranched block with cross-links or functionalities on the dendritic ends. Each dendritic block has 16 reactive sites, hence there are 32 possible cross-links or anionic functionalities per DLD structure. Three different DNGs were used, named DNG1−3, where DNG3 has more anionic charges per building block (22/32) than DNG2 (20/32) and DNG1 (12/32). The remaining reactive sites are cross-links in all cases. DNG1 is thus more cross-linked and less charged than DNG3.

As mentioned above, the network architecture of the DNGs is not known, but zeta potential measurements indicate a PEG palisade with internalised anionic moieties. The size of the gels is too large for there to be a single anionic core, meaning that a gel has several anionic cores with a PEG corona, see *Figure 5*. PEGylation has long been a popular way to increase biological stealth and circulation times for nanoparticles in drug delivery.[129,130] In addition, PEGylation has been reported to decrease toxicity and increase stability of the PEGylated species.[44,131] In recent years, several research groups have raised concerns regarding PEG antibodies for PEGylated formulations and nanoparticles.[132–134] It is of high importance to investigate what physiological responses these antibodies will cause.[135] However, it is worth noting that there are still new reports of promising PEGylations.[108,136]

1.3 Model membranes

Model membranes are often used when evaluating AMPs and carrier systems due to the complexity of bacterial and cell membranes.[137] The lipid bilayer composition of the cell walls differs greatly between bacterial strains, cell types and growth conditions used,[138] providing varying environments for AMPs to act on, see *Figure 6*. The main difference in bacteria is between Gram-positive and Gram-negative bacteria, see *Figure 7*.

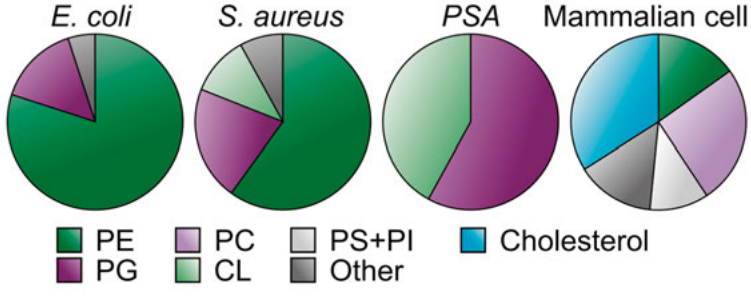

Figure 6. Lipid composition of the membranes of different bacterial strains[139] and the mammalian plasma membrane.[140] *E. coli: Escherichia coli, S. aureus: Staphylococcus aureus, PSA: Pseudomonas aeruginosa,* PE: Phosphatidylethanolamine, PG: Phosphatidylglycerol; PC: Phosphatidylcholine, CL: Cardiolipin, PS: Phosphatidylserine, PI: Phosphatidylinositol, and Other: lipids present in minor amounts.

Gram-positive bacteria have a single membrane protected with a thick layer consisting of a peptidoglycan/teloic acid polymer network.[141] Gram-negative bacteria do not have this polymer network; instead, they have two membranes with a peptidoglycan layer in between.[142] The outer membrane is covered in lipopolysaccharides coupled to the membrane by Lipid A. Due to this structural difference, it follows that some AMPs are selective for either Gram-positive or Gram-negative bacteria.[143–145]

Apart from the structural differences, there are also differences in the phospholipid composition of the lipid bilayers (see *Figure 6*) and in the membrane protein content. Membrane proteins can constitute up to 50% of the weight of bacterial and cell membranes, and are essential for transport, recognition and function.[146] Some membrane proteins have carbohydrates attached that both act as protection for the cell and are essential for cell interactions, further increasing the complexity.[147]

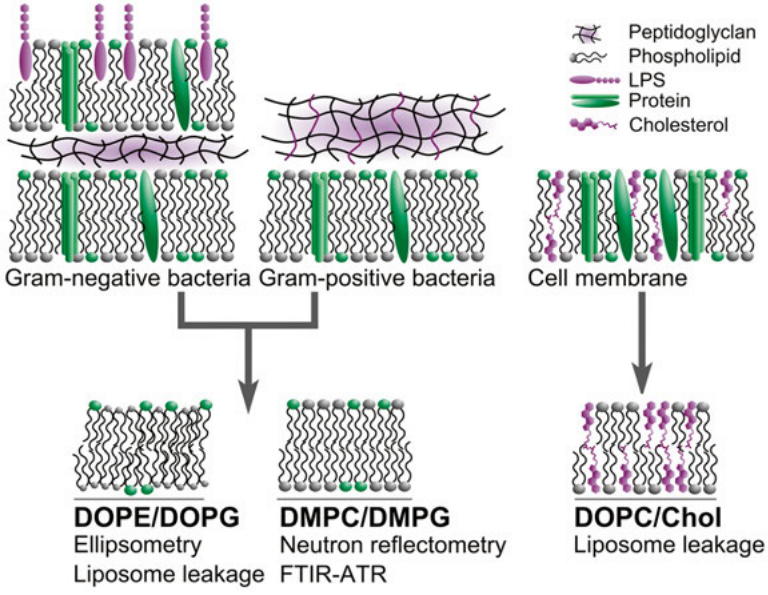

Figure 7. (Top left) A Gram-negative bacterial membrane, purple tails in the outer membrane illustrating lipopolysaccharides (LPS) and the purple net in between the lipid bilayers illustrating the peptidoglycan layer. (Top centre) Gram-positive bacterial membrane with one lipid bilayer and a thick outer peptidoglycan layer. (Top right) Mammalian cell membrane with cholesterol (purple) and lacking a peptidoglycan layer. At the bottom, the different bilayers used in this thesis are presented, together with the analysis techniques applied. The model membranes used are simplified models highlighting certain properties of the modelled membrane, which is important to keep in mind when interpreting the results.

Investigating AMP interaction directly with a bacterial or cell membrane can therefore be challenging. When developing a drug delivery system and investigating the mechanism of interaction, it can be useful to turn to simpler models as initial tools for evaluation before moving on to real biological membranes and *in vitro* studies. These model membranes are lipid bilayers, often containing two or three of the most characteristic lipids for the membranes in question.[148–150] This approach enables a compromise between obtaining membrane-specific information and keeping the models simple enough to deduce the effects of different components. By varying the lipid composition, one can tune the properties of the bilayer to fit the desired purpose. This can be to model a certain bacteria or cell, highlight a certain property, e.g., charge, or suit a certain analysis method, e.g., neutron reflectometry.

There are many studies of the lipid composition of bacterial membranes, with a considerable variation in the results depending on the bacterial strain studied and the growth conditions used.[138,139] The lipid composition of the bacterial membrane will change with pH, oxygen and nutrient availability, as well as with temperature.[151] The majority of bacteria have the negatively charged

phosphatidylglycerol (PG) lipid in their membranes, see *Figure 6*. The proportion of charge varies between strains. For example, *E. coli* have approximately 15% anionic PG in their membranes and 80% zwitterionic phosphatidylethanolamines (PE).[139] For cationic AMPs, the anionic PG is an important factor for electrostatic attraction and interaction enabling membrane binding and disruption. To emphasise the importance of electrostatics for AMP/membrane interactions, a 3:1 molar ratio of zwitterionic:anionic components was chosen as a suitable model for a charged membrane. Unsaturated DOPE or saturated DMPC was used for the zwitterionic component, while unsaturated DOPG or saturated DMPG was used for the anionic component depending on the analysis technique used, see *Figure 7*. DOPE/DOPG bilayers have the advantage of being more biologically relevant, as PE is much more common in bacteria than PC, see *Figure 6*. DOPE/DOPG lipids are suitable for liposome leakage experiments as well as bilayer experiments using QCM-d, FTIR-ATR and ellipsometry. However, the difference in head group and tail volume and thereby packing parameters between PE and PG tend to give uneven bilayers.[152,153] This is not a problem, unless roughness on the low Ångström level is required, which is the case for neutron reflectometry. In this case, more even bilayers and better resolution can be achieved by using DMPC/DMPG (3:1 mol/mol) bilayers with similar head group sizes instead. The tail-saturated DMPC/DMPG lipids are also stable and commercially available in deuterated form, which improves contrast in neutron reflectometry.

Mammalian cells have a different lipid composition as compared with bacteria, see *Figure 6*. For example, cholesterol is a rare component in bacterial membranes, but composes up to 45% of eukaryotic cell membranes.[154] The charge of the membrane also differs, eukaryotic membranes are largely composed of zwitterionic lipids, such as DOPC, resulting in a close to neutral potential.[155] Bacteria, on the other hand, have a larger proportion of anionic lipids, such as DOPG, yielding a negative potential. Using DOPC and cholesterol in a 3:2 molar ratio to model mammalian cells is a way to emphasise these two clear differences between bacteria and mammalian cells.[149,154,156] The DOPC/cholesterol model is suitable for studies on both liposomes and supported bilayers.[50]

2. Aims and scope

Antimicrobial resistance is a pressing issue. AMPs have received considerable attention as a possible alternative way to treat resistant bacterial strains. The opportunities that AMPs offer also come with formulation challenges, including peptide toxicity, high cost-of-goods and proteolytic sensitivity. Peptide carrier systems are used to meet these challenges.

Earlier studies have mainly focused on model peptides, each highlighting a certain property (e.g., secondary structure or charge), as mentioned in Section 1.1. This thesis mainly uses active AMPs and their derivatives, resulting in a more complex system. Based on extensive background knowledge about peptide/microgel interactions in the 100 µm range, the aim of this project was to utilise microgels in the 100 nm (0.1 µm) range. Both erodible MAA microgels and degradable DNGs were evaluated as possible peptide carriers.

The aim of this thesis was to evaluate how MAA microgels and DNGs perform as AMP carriers from several perspectives (as illustrated in *Figure 8*):

- Evaluation of factors affecting peptide loading and release to/from MAA microgels (Papers I, II and IV) and DNGs (Paper V), including peptide stability upon exposure to proteolytic enzymes (Papers II and V).
- Understanding how AMP loading onto MAA microgels (Papers II and III) and DNGs (Paper V) affects interaction with bacteria membrane models.
- Evaluation of the antimicrobial activities of AMP-loaded MAA microgels (Paper II) and DNGs (Paper V), how these correlate with membrane interactions in model lipid membranes, and how they depend on peptide loading and release.
- Evaluation of toxicity of AMP-loaded MAA microgels (Paper II) and DNGs (Paper V) towards erythrocytes, and their interaction with mammalian membrane models.

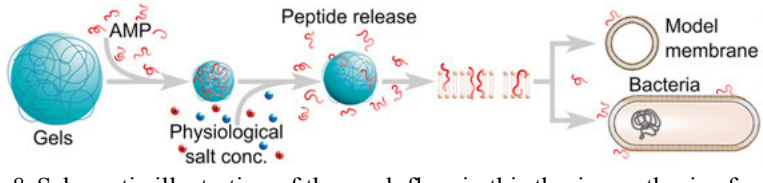

Figure 8. Schematic illustration of the work flow in this thesis: synthesis of gels, peptide loading and release, and study of membrane interactions.

3. Methods

3.1 Microgel synthesis

The MAA microgels were synthesised by starved-feed emulsion polymerisation using an oxygen radical initiator, see *Figure 9*, as previously reported by Saunders and Rodriguez.[90,157] Emulsion polymerisation is a technique where vigorous mechanical stirring and a surfactant are used to keep the monomers in small emulsion droplets throughout the propagation of the network. A water soluble initiator is used and the propagation of the network occurs within surfactant micelles. This restricts the microgel growth, yielding a narrow size distribution and minimising the risk of macrogel formation. Starved-feed is a technique where a set monomer mixture is continuously fed to a reaction mixture at such rate that most monomers are consumed before more are added. This facilitates an even monomer distribution throughout the gel, even when one component is favoured in the reaction.[158] The size of the gels in the reaction mixture was followed by photon correlation spectroscopy (PCS), as described under Section 3.2; when the gel size reached 120 nm, the reaction was quenched by cooling. To remove unreacted monomers, buffer and initiator, the reaction mixture was excessively dialysed against Milli-Q water.

These microgels, in the nanoscale range, are smaller than the wavelength of visible light and impossible to see with the unaided eye or light microscopes. There are, however, numerous techniques that can be used to visualise such particles; the ones below are those utilised in this thesis.

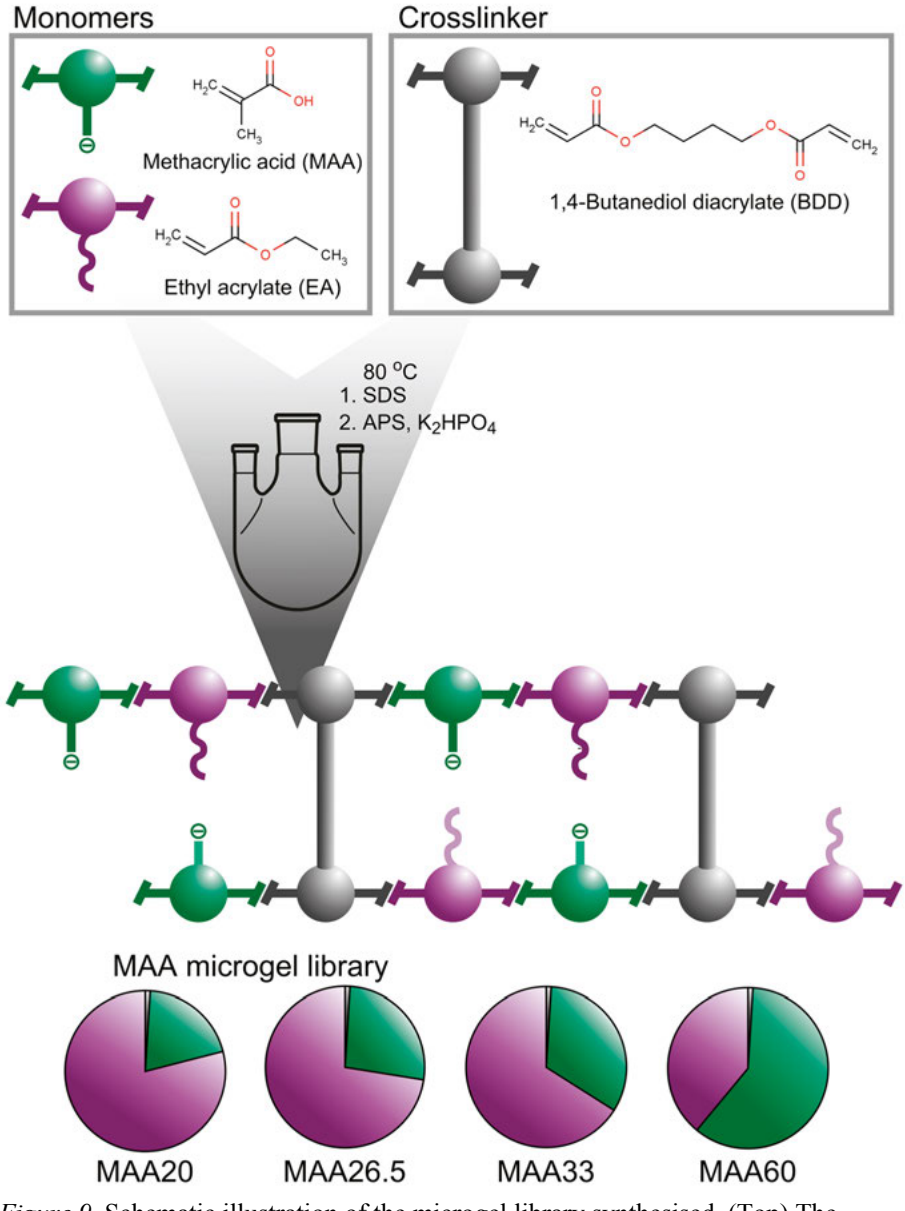

Figure 9. Schematic illustration of the microgel library synthesised. (Top) The chemical structure of the monomers used. (Middle) The reaction conditions used. SDS (sodium dodecyl sulphate) is a surfactant keeping the monomer mixture in small droplets, APS (ammonium persulfate) is an oxygen radical initiator, K_2HPO_4 buffers the system. The pie charts on the bottom illustrate the monomer composition in wt% for the microgels used in this thesis, with ethyl acrylate in purple, meth-acrylic acid in green and the cross-linker in grey (1 wt%).

3.1.1 Cryogenic transmission electron microscopy (cryo-TEM)

A diluted solution of gels in buffer is applied to a grid, forming thin water menisci. The water is rapidly cooled using liquid ethane (-165 °C) to force the water molecules to form amorphous ice. An electron beam is directed through the sample and its interaction with nuclei in the sample is used to obtain an image of the microgels.[159] The short wavelength of the electron beam enables a high resolution visualisation of particles in the nano-range. Advantages of cryo-TEM include the small sample volumes required (µL) and the possibility to visualise individual particles in their hydrated native state in solution.[160]

3.1.2 Scanning electron microscopy (SEM)

SEM was employed to visualise surface-bound microgels. An electron beam is focused on the sample and secondary emitted electrons are detected and used to visualise the sample.[161] SEM requires dry samples in vacuum. This is a drawback for microgels, as the polymer network collapses under dry conditions. Environmental SEM has been developed in later years to enable the use of SEM at higher humidity.[162,163]

3.1.3 Atomic force microscopy (AFM)

AFM uses a nano-sized tip to scan a surface, yielding information on topography, force and mechanical properties. The properties and topography are extracted from the change in amplitude when the oscillating tip comes close to the material, and is affected by tip-sample interactions. It is important to keep in mind that the results obtained depend on the size of the tip, the force with which the tip hits the sample, as well as the user-set value to define contact with the sample.[164] In our case, the measurements were performed on surface-bound microgels in solution using PeakForce tapping mode, yielding information on both the topography of the sample and quantitative nanomechanical property mapping (QNM).[165]

3.1.4 Fourier transform infrared (FTIR) spectroscopy

FTIR spectroscopy was used to monitor network degradation of DNGs. Infrared light has the same energy range as the vibration of covalent bonds and is particularly effective for detecting and studying functional groups. DNGs were diluted in buffer and kept at 37 °C. Samples were taken out of the solution in a time-resolved manner, immediately frozen in liquid nitrogen and subsequently freeze-dried. The dry residue was analysed using FTIR spectroscopy, monitoring the intensity decay of the ester carbonyl stretching band.[166] As the dendritic blocks of the DNGs are hydrolysed, the amount of ester bonds will decrease, as will the intensity of the corresponding ester carbonyl band.

3.2 Peptide loading and release

3.2.1 Size determination

The gel size decreases upon AMP loading onto microgels, this is due to both the decreased electrostatic repulsion and the entropic gain of releasing counterions upon peptide-microgel binding, which makes it favourable for the gels to adopt a more compact conformation. Two convenient methods for size determination of gels in solution are photon correlation spectroscopy (PCS), also called dynamic light scattering (DLS), and nanoparticle tracking analysis (NTA). Both techniques use Brownian motion to determine the hydrodynamic radius of particles. PCS is based on the translational diffusion coefficient to obtain the hydrodynamic particle size using the Stokes-Einstein equation.[167] Since the equation assumes a hard sphere in the size calculation, the technique is sensitive to the concentration, turbidity, fluorescence, colour and shape of the particles.[168] In the case of polymer hydrogels, dilute polymer chains with their efficient hydrodynamic screening can affect the determined size. PCS has a tendency to over-represent larger particles in a population and thereby overestimate particle size, hence the best suited samples are monodisperse ones.[168] NTA also uses the translational diffusion coefficient and the Stokes-Einstein equation. Unlike PCS, which reports on an ensemble average, NTA records particle mobility of individual particles in a sample using a CCD (charge coupled device) in real-time,[169] enabling studies of particle concentration, aggregation and size distributions.[170]

3.2.2 Zeta potential

When working with charged polymer networks and oppositely charged AMPs, zeta potential is a convenient method of monitoring changes of the potential as AMPs are loaded onto the microgel. It can give information on peptide localisation; a peptide in the gel core does not affect the zeta potential whereas a peptide attached to the gel surface will, see *Figure 10*.

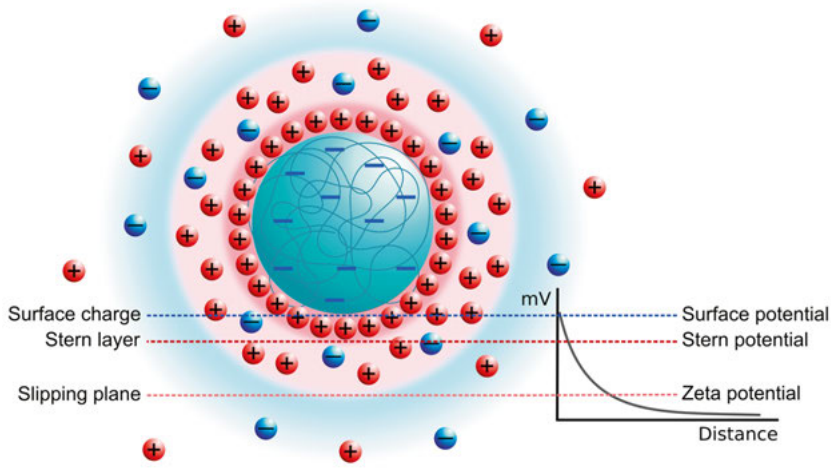

Figure 10. Schematic illustration of a dispersed microgel and the ions in solution associated with it. The graph (right) illustrates the potential difference as a function of distance from the particle surface, indicating the difference between surface potential, stern potential and zeta potential. The illustration is an adapted original.[171]

Maintaining a high charge of either sign has been reported to increase the colloidal stability and decrease the risk of aggregation.[172] Unless the particles studied are hard and monodisperse, the zeta potential is not an absolute measure of the potential of a particle. Rather, it is the potential difference between the surrounding buffer and the stationary layer of liquid attached to e.g. the microgel at different peptide loads, see *Figure 10*. It is measured, e.g., using a DLS apparatus with a cuvette equipped with electrodes, allowing an electric potential to be applied over the sample. The zeta potential can then be calculated using the particle electrophoretic mobility and the Helmholz-Smoluchowski equation.[168,173] This parameter is diffuse for uneven soft particles such as the studied microgels, and the zeta potentials should not be used as absolute values, but taken as effective zeta potentials and compared with samples containing the same particles.[174]

3.2.3 Quantification of peptide loading in microgels

In the present work, both confocal microscopy and ellipsometry were used to quantify peptide loading to MAA microgels. Both of these techniques utilise microgels covalently immobilised on a surface, using either silica wafers (ellipsometry) or glass cover slips (confocal microscopy) as substrate. The chemistry behind obtaining these microgel coatings is a silanisation followed by a reaction between an epoxy group and a carboxylic acid in the microgel, as illustrated in *Figure 11*.[102,175]

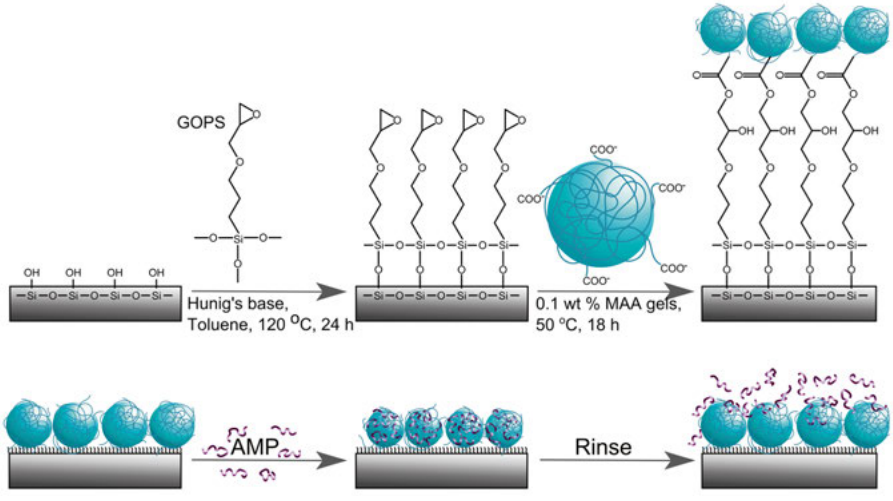

Figure 11. (Top) Scheme of 3-glycidoxypropyltrimethoxysilane (GOPS) silanisation and covalent coupling of the carboxylic acids of the microgel to the introduced epoxide functional groups at the interface. The GOPS-functionalisation minimises the number of exposed silanol groups and thereby decreases the risk of background peptide adsorption. (Bottom) Illustration of peptide loading and release.

The reaction yields an approximately 10% surface coverage of microgels, as determined using both AFM and SEM. The GOPS surface modification minimises the number of exposed silanol groups at the interface and thereby the background adsorption of peptides. By minimising the background adsorption and always presenting the peptide loading to microgels in comparison with the background adsorption, it is possible to obtain a measure of the peptide loading and release to/from immobilised microgels, see *Figure 11*.

In confocal microscopy, fluorescently marked peptides (Alexa488) were loaded onto microgels and the surfaces were visualised in a confocal Leica DM IRE2 laser scanning microscope (Leica Microsystems, Wetzlar, Germany). This technique visualises different parts of a sample through focusing on different confocal planes along the z-direction, perpendicular to a glass surface on which the sample is mounted, e.g., surface-immobilised microgels loaded with fluorescently marked peptides, see *Figure 12*.[176]

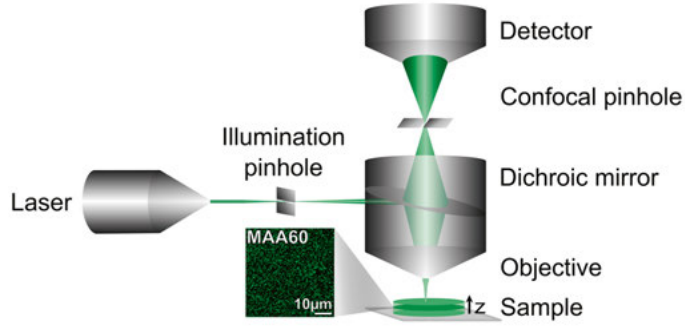

Figure 12. Schematic of a confocal microscopy set-up. A confocal microscope enables visualisation of a single plane in the z-direction of the sample. The example image to the right is of surface-immobilised MAA60 microgels loaded with P-Lys.

To obtain a value of the peptide loading, the average intensity of three random 150 μm^2 squares was measured using Image J software (National Institutes of Health, Bethesda, U.S.A.).[102,177] This is not the fluorescence intensity from a single gel, but instead an average over many gels. It is important to keep in mind that conjugating a peptide with a hydrophobic fluorescent label can affect the peptide properties and thereby the peptide/microgel interactions.

In ellipsometry, unmodified peptides were used in an experimental set-up, as described in *Figure 13*. The mass change at the gel surface was monitored time-resolved, using null ellipsometry with a refractive index increment of 0.154 cm^3/g.[178,179]

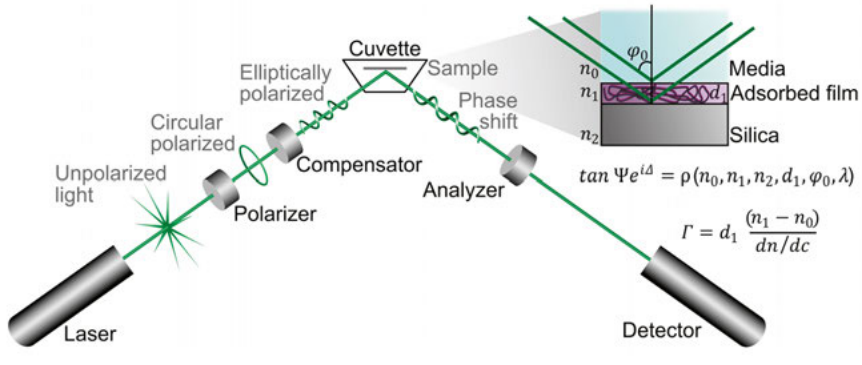

Figure 13. Ellipsometry set-up. The adsorbed film changes the refractive index of the surface, causing a phase shift in the angle and amplitude of the elliptical light. Through measuring Ψ related to the amplitude difference after reflection and Δ describing the phase shift after reflection, the adsorbed amount (Γ, mg/m^2) can be modelled using the thickness of the adsorbed film (d_1), the refractive index of film and substrate (n_x) and the refractive index increment of the adsorbing film (dn/dc). The refractive index increment is an approximation depending on the component adsorbed.[178,179]

Bicinchoninic acid (BCA) assay was used for quantification of peptide loading to DNGs. The DNGs have a PEG corona, and are therefore not easily attached to silanised surfaces, as mentioned above. In addition, their degradability makes it difficult to study peptide binding to a gel-covered surface in a reliable way. Hence, the solution-based BCA assay was used instead. The latter uses Cu^{2+} ions that are reduced to Cu^{+} by peptide bonds as well as tyrosine, cysteine and tryptophan side-chains.[180] BCA then forms purple complexes with Cu^{+} that can be detected through absorbance at 562 nm.[180]

A schematic of the BCA assay is presented in *Figure 14*. In short, DNG and a known excess concentration of AMP were allowed to equilibrate, after which unbound peptide was removed by centrifugation through 10kDa cut-off filters. To account for peptide-filter binding, the same type of filters was used to obtain the calibration curve. The samples and calibration curve were developed using BCA and the amount of bound peptide was calculated from the absorbance difference between the known concentration added to the gels and the peptide concentration in the filtrate.

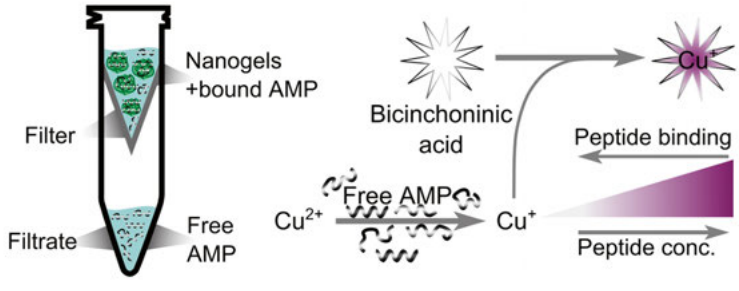

Figure 14. Schematic of BCA assay. (Left) DNGs are mixed with a known concentration of AMP, the unbound peptide is filtered off and quantified using BCA assay. The amide bonds in the peptide reduce Cu^{2+} to Cu^{+}, which forms a coloured complex when mixed with bicinchoninic acid. The complex can be quantified using absorbance at 562 nm, and a calibration curve.[180]

3.2.4 Conformation of microgel-bound peptides

The techniques above focused on the microgels or the amount of peptide loaded from a quantitative perspective. It is also interesting to see how a peptide interacts with the microgel in terms of peptide conformation. Two techniques were utilised for qualitative study of AMP-gel interactions: nuclear magnetic resonance (NMR) spectroscopy and circular dichroism (CD) spectroscopy.

CD is a technique where chiral molecules interact with circularly polarised light.[181] The spectra produced show the difference in adsorption of left- and

right-handed polarised light. It is well-known that α-helix-forming peptides have a characteristic CD spectrum that is different from that of peptides in random coil.[182–184] Examples of CD spectra, along with the equation used for calculating the α-helix content, are presented in *Figure 15*. Monitoring the peptide conformation is a way to verify membrane or microgel interactions of α-helix-forming peptides. [38,50] A presence of colloid particles such as microgels and liposomes in the studied samples often introduces noise through light scattering at wavelengths below 200 nm.[185] The method of calculating α-helix content from CD data was selected to exclude these wavelengths.

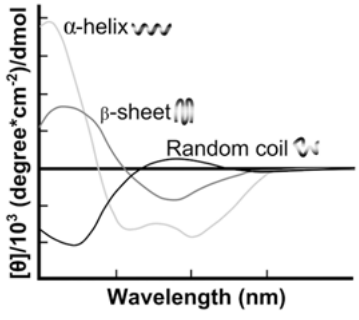

$$X_\alpha = \frac{A - A_{rc}}{A - A_\alpha}$$

Figure 15. Examples of CD spectra for different peptide conformations (left) and the equation used for calculation of α-helix content (right). The α-helix content (X_α) of a sample can be calculated using the CD signal from the sample at 225 nm (A), and from references with 100% α-helix (α) and 100% random coil (rc), respectively.

NMR spectroscopy is a technique using radiofrequency pulses and atomic spins in a magnetic field to investigate the chemical surroundings of atoms both inter- and intra-molecularly.[83] In this thesis, NMR spectroscopy has been used to elucidate the peptide 3D structure upon microgel binding. Depending on the experimental set-up and the pulse sequences used, a wide range of information can be obtained. A variety of 2D NMR experiments provides information on nuclear connectivity via covalent bonds or through space: TOCSY (Total correlated spectroscopy) shows which protons are part of the same spin system and NOESY (Nuclear Overhauser Effect Spectroscopy) gives information on spins that are close in space via the Nuclear Overhauser Effect (NOE), whereas *tr*NOESY gives time-resolved information on spins close in space, hence the folding dynamics of a molecule, e.g., a peptide. Such experiments were used to determine the inter-proton distances needed to calculate the 3D structure using the CYANA 2.1 software.[186] An ensemble structure was generated using the 20 lowest energy conformations; the structure was analysed using the PyMol,[187] MOLMOL[188] and Chimera softwares.[189]

In saturation transfer difference (STD) NMR spectroscopy, a chosen signal is saturated. As the peptide moves, the saturated spins will interact with protons in its surroundings, resulting in altered signal intensities for those spins and

producing signals in the STD spectra.[190] This technique was used for binding site mapping[191,192] to find the amino acids closest to the polymer network of the microgel. A saturation at -4 ppm was used to target the microgel while avoiding any direct saturation of the free peptide.

3.3 Membrane interactions

Model membranes of bacteria and cells were used in this thesis as a way to study the efficiency, toxicity and mechanisms of interaction of microgels and AMPs. There is a battery of techniques that can be used when studying model lipid bilayers.

Liposome leakage: By preparing liposomes incorporated with carboxyfluorescein (CF) at a self-quenching concentration, membrane interaction can be monitored through measuring the fluorescence from a liposome/AMP/microgel sample at 517 nm time-resolved, see *Figure 16*. Released AMP disrupts the liposomes and causes CF to leak and be diluted, suppressing self-quenching and resulting in increased fluorescence. By disrupting all liposomes in the system at the end of the experiment with a surfactant (Triton) and comparing with the fluorescence from the sample, one can obtain the liposome leakage as a percentage of disrupted liposomes. This value can be compared between drug delivery systems, peptides and concentrations.[193,194]

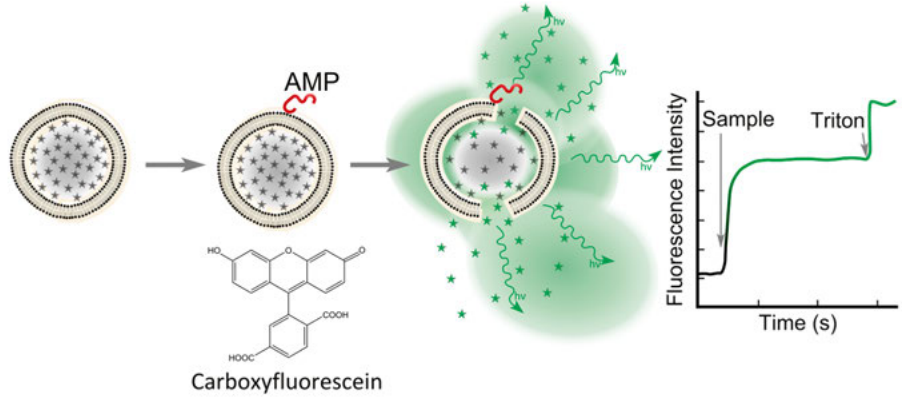

Figure 16. (Left) Illustration of the principle behind liposome leakage studies. Liposomes incorporated with CF at a self-quenching concentration (grey stars). (Centre) The AMP disrupts the liposomes and CF leaks out and is diluted to fluorescent concentrations by the surrounding buffer media (green). (Right) Example measurement with fluorescence intensity vs. time; sample and Triton (surfactant) addition indicated by arrows. (Bottom) Molecular structure of the fluorophore used.

Supported bilayers in ellipsometry: Model lipid bilayers can be deposited on a silica surface and used for monitoring AMP/drug delivery system-binding in ellipsometry, see *Figure 17*. To achieve this, liposomes with a diameter of 50 nm were prepared by extrusion[50,195] and subsequently added to an ellipsometry cuvette with a silica surface pre-treated with poly-L-lysine. The poly-L-lysine pre-treatment is performed at low ionic strength for flat lysine binding, resulting in charge reversal.[196] This facilitates liposome binding/rupture, and suppresses background adsorption of peptide onto any bilayer defects.[197] The small liposomes rupture on the surface and a bilayer is formed through vesicle fusion.[149,198] A lipid bilayer with full coverage corresponds to ~4.4 mg/m^2 depending on the lipids used, assuming a refractive index increment of 0.154 cm^3/g.[178,179,199] Excess lipids are removed through extensive buffer rinsing. The sample is then added to the bilayer and the dry-mass change on the lipid bilayer is monitored time-resolved upon addition of sample and during rinsing with buffers of different ionic strengths. A schematic ellipsometry bilayer experiment is presented in *Figure 17*.

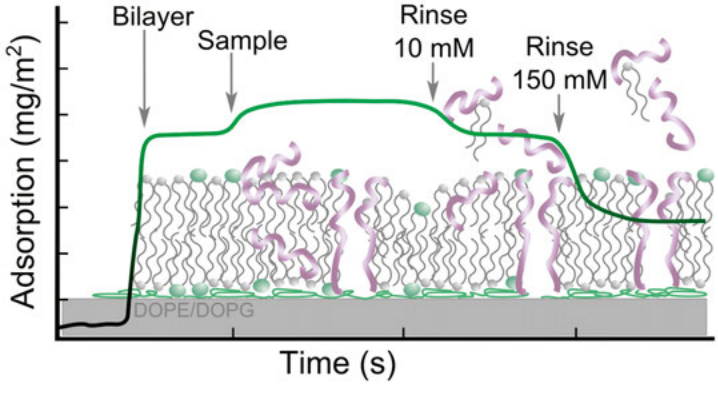

Figure 17. Schematic illustration of an ellipsometry bilayer experiment. A lipid bilayer is formed on the surface through vesicle fusion,[200] as shown by the rapid increase in adsorbed mass. An AMP sample is added and the peptide adsorbs and inserts into the bilayer, increasing the mass further. Rinsing with low and high ionic strength buffers removes weakly adsorbed peptides and loose lipids. In this example, the peptide caused severe membrane defects and lipid removal, resulting in a lower mass than the initial bilayer.

Supported bilayers in neutron reflectometry (NR). NR is another technique for studying lipid bilayers, providing information on structure and composition perpendicular to the silicon crystal surface that supports the bilayer.[201,202] Neutrons have zero charge and therefore interact with matter only via nuclear forces.[203,204] Since nuclei are small, the probability for neutron absorption and reflection is low, enabling the neutron beam to penetrate long distances into materials, giving structural information from deep within samples before all neutrons are absorbed or reflected, see *Figure 18*.[205]

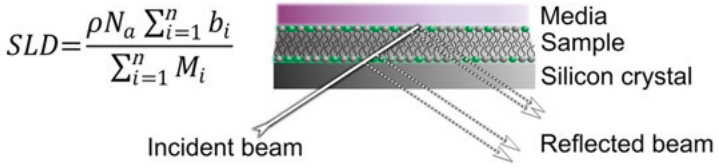

Figure 18. (Left) Equation for calculating SLDs for materials and molecules where: ρ – material density, N_a – Avogadro's number, b_i – neutron scattering length and M_i – atomic molar mass of the *i*:th element. (Right) Illustration of the neutron beam going through the silicon crystal and sample and being partially reflected.

Different nuclei have different properties (e.g., spin and energy levels) which affect their interactions with neutrons and give each element and isotope their own neutron-scattering length, *b*. Knowing the neutron-scattering length of nuclei enables calculation of the scattering length density (SLD) of a molecule or material, using the equation in *Figure 18*. Knowing the SLDs for peptide, lipids and drug carrier systems enables modelling of the NR data.[206] The isotopes hydrogen and deuterium have different *b*s, and consequently the solvents H_2O and D_2O have different SLDs. By varying the composition of deuterated and hydrogenated buffers, or through selective deuteration of the sample, it is possible to highlight different aspects of your system, as exemplified for peptide interactions with a deuterated lipid bilayer in *Figure 19*.[207] NR is therefore a powerful technique for obtaining structural information of biologically relevant systems.[208]

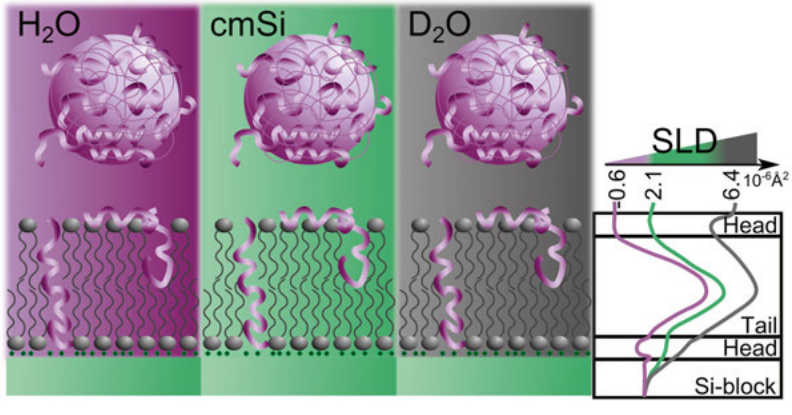

Figure 19. Illustration of how changing the contrast of the media highlights different aspects of the bilayer system in neutron reflectometry depending on the scattering length density (SLD) of the materials and molecules used; deuterated lipids in grey, silicon crystal in green and hydrogenated peptides and microgels in purple. (Left) Using deuterated lipids highlights the lipid bilayer in the h-contrast. (Centre) When the media is contrast-matched to silicon (cmSi), the surface underneath becomes invisible and peptides, lipids and microgels are highlighted. (Right) In the d-contrast, the hydrogenated microgels and peptides are most visible. By modelling these three contrasts together, a reliable picture of peptide interactions and the membrane defects created can be obtained.

NR data are modelled as layers; each with an SLD, thickness, roughness and hydration. When studying a bilayer in NR it is therefore important to choose lipids that can form flat confluent bilayers, in order to minimise roughness and obtain as high resolution as possible.[209] In Paper III, deuterated DMPC/DMPG lipids were used to obtain a better contrast when studying the interaction with a hydrogenated peptide. Using a hydrogenated lipid would make the SLDs of peptide, microgel and lipid too similar and the change in reflectivity would be small and difficult to model. By looking at the system in three different contrasts (hydrogenated buffer, buffer contrast-matched to the silicon substrate underneath the lipid bilayer, and deuterated buffer), different aspects of the peptide/microgel/bilayer interaction can be highlighted, including the formation of solvent-filled pores, microgels present on top of the bilayer, or lipid removal, see *Figure 19*.

For a typical NR experiment in this study, liposomes of deuterated DMPC:DMPG (3:1 mol/mol) were prepared through tip-probe sonication, mixed with a Ca^{2+} solution and introduced to the silicon crystal by manual injection. A lipid bilayer was formed through vesicle fusion and characterised in the three contrasts mentioned above. Microgel-AMP sample was prepared in Milli-Q water, diluted 1:10 in Tris (50 mM, pH 7.4, 150 mM NaCl) buffer, equilibrated overnight for peptide release and subsequently pumped into the neutron cell. After 30 min incubation, the sample was rinsed and the bilayer characterised again in three contrasts to determine the bilayer structure after peptide interaction.[210] The neutron data was modelled using RasCal.[211]

Supported bilayers in attenuated total reflection – Fourier transform infrared spectroscopy (ATR-FTIR). ATR-FTIR is a technique that analyses the IR response from a sample close to a surface.[212,213] The beam is reflected at the boundary between the crystal and the sample or medium in contact with it, but while doing so it protrudes into the medium. Through reflection, a longer sample path is obtained, yielding enhanced signals from low-concentration species, *Figure 20*.[214] This technique provides information on the chemical interactions as an AMP is introduced to a bilayer, which conformation the peptide has, as well as which amino acids interact with different parts of the lipid bilayer.[213,215,216] The bilayer is prepared and introduced in the same way as for neutron reflectometry, as described above. The IR signal over time monitors changes upon microgel/AMP interactions.

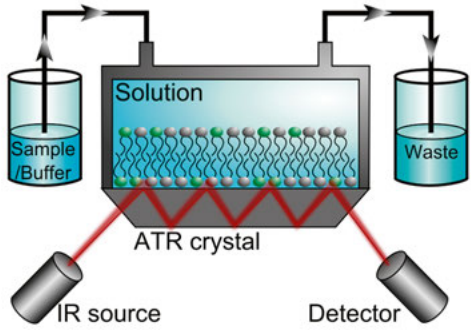

Figure 20. Schematic illustration an ATR-FTIR set-up. The IR beam passes through the sample several times before it reaches the detector, enhancing weak signals. Sample and buffers can be pumped in and out of the cell, enabling rinsing and introduction of AMP/microgel samples.

3.4 *In vitro* effect studies

Several *in vitro* tests were performed in order to evaluate the MAA microgels and DNGs as AMP carriers. For evaluation of antimicrobial activity, minimal inhibitory concentration (MIC),[217] viable count analysis (VCA)[63,107] and radial diffusion assay (RDA)[38] were utilised.

MIC is a time efficient technique suited for screening of antimicrobial activity on many bacterial strains, since several strains can be tested in parallel in multiwell plates. The result obtained is the concentration of peptide required to kill a determined amount of bacteria of a certain strain within a certain incubation time. These analyses were performed using both standard strains (methicillin-resistant *staphylococcus aureus, MRSA; E. coli* and *Pseudomonas aeruginosa, PSA ATCC*) and a clinical isolate (*clin. PSA*). Visual inspection after 24 h was used to determine the concentration of peptide that completely inhibited bacterial growth.[50]

VCA of *E. coli* was performed by incubating bacteria with microgel-AMP formulation for 16 h and thereafter counting the number of colony-forming units (CFU) as a function of AMP concentration.[107]

RDA is a technique where microgel/peptide formulation is applied in a well in an agar plate with bacteria growth (in this case *E. coli*) and the antimicrobial effect is evaluated as the radius of inhibited growth around the well with AMP-microgel formulation.[38] The agar matrix hinders microgel, but not free peptide diffusion. Thus, this is a test of the effect of released peptide, showing both if the peptide is intact after microgel loading and if it is released in a high

enough concentration to be bactericidal. Worth noting when comparing different peptides is that they can interact differently with the growth media, thus affecting the radii of inhibited growth differently.

Hemolysis experiments were performed to get an indication of cell toxicity. The erythrocyte lysis caused by peptides and microgels is used as a measure of toxicity. The proportion of lysed cells is measured through hemoglobin absorbance at 550 nm and compared with a reference sample with 100% lysed cells (2% Triton).[50] Even if the results are promising, it is important to remember that erythrocytes are just one cell type. To draw conclusions about the biocompatibility and safety of these peptide carrier systems, extensive *in vitro* and *in vivo* tests would be required.

Since several AMPs are sensitive to proteolytic activity, there is a risk of AMP degradation and subsequent activity loss. To investigate potential protective effects of microgels, free and microgel-loaded AMPs were exposed to *Pseudomonas elastase (PSA elastase),* a key infection-related proteolytic enzyme.[50,218] It is worth noting that infected tissue is characterised by high activity of both bacterial and cell proteolytic enzymes.[52,219] After treatment with enzyme, gel electrophoresis was used to determine the ratio of intact peptide through Coomassie brilliant blue staining.[218]

4. Results and discussion

4.1 Microgel synthesis

MAA microgels were synthesised by inversed emulsion polymerisation, as described previously.[90,122] Since the gels were synthesised using a radical reaction, the charge densities of these gels were determined by titration. The results in Papers I and II showed that the reaction favoured MAA, making the acid content of the microgels slightly higher than that of the feed solution used, see *Table 2*. The pK_a values of these gels were between 6 and 7 (titration data), which is higher than what is expected from an isolated carboxylic acid. This can be explained by the intrapolymer interactions present in charged polymers, resulting in a smearing out of the titration, as commonly observed for polyelectrolytes.[220] Thus, the MAA microgels are responsive around physiological pH, which is of interest when evaluating these microgels as possible AMP carriers. The gels showed dramatic volume changes as a function of pH, swelling to three times their diameter as measured using PCS, see *Table 2* and *Figure 21A*.

Table 2. Data on the synthesised microgels including MAA content and pK_a values from titration data, size at physiological pH, swelling ratio and ionisation degree at physiological pH. Gel compositions and abbreviations are explained in *Figure 9*.

Microgel	% MAA[a]	pK_a[a]	Size at pH 7.4 [nm][b]	Swelling ratio[c]	Ionisation at pH 7.4[a]
MAA20	22.1±1.1	7.0	174±2	2.4	0.72
MAA26.5	34.3±1.1	6.9	236±1	3.1	0.76
MAA33	36.9±0.4	6.4	265±2	3.3	0.91
MAA60	63.3±1.5	6.5	338±1	2.7	0.89

The effective zeta potentials of all four MAA microgels used in this thesis were equally low at -30 mV, see *Figure 21B*. A high zeta potential of either sign is often argued to indicate good colloidal stability.[221] Cryo-TEM images were taken of the MAA33 gels to visualise the systems in an aqueous environment, as can be seen in *Figure 21C*. The microgels are loosely cross-linked

and have a low contrast in cryo-TEM. The toxicity of the microgels was evaluated through hemolysis. Despite the high acid content of the gels, the hemolysis was low, even up to a high 500 ppm MAA microgel concentration, see *Figure 21D*. This is a promising result from a biocompatibility perspective.

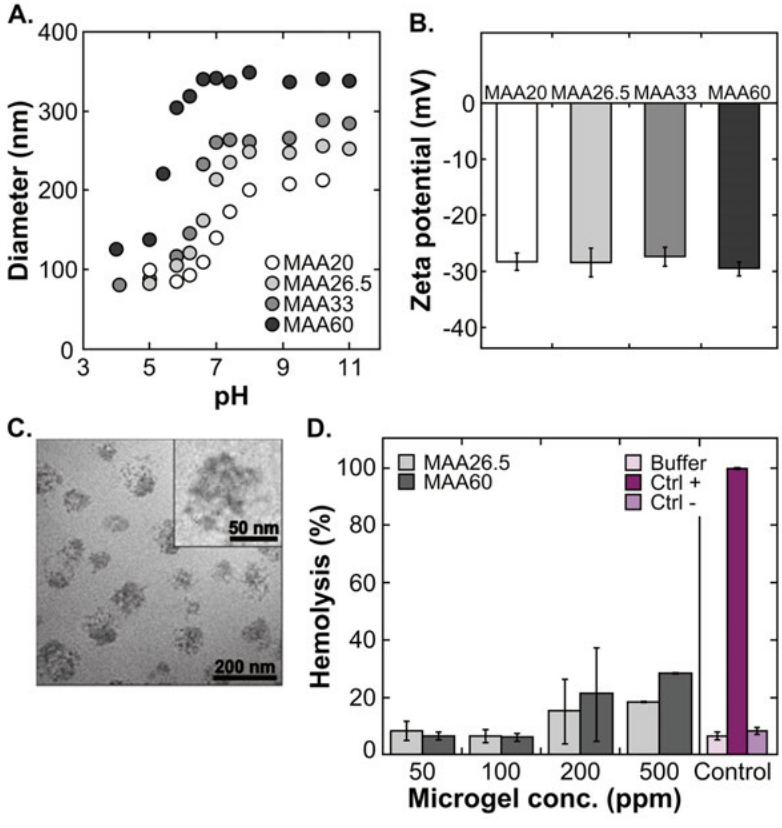

Figure 21. (A) Microgel size as a function of pH, in 100 mM buffers. (B) Effective zeta potential as a function of microgel charge in Tris (10 mM Tris, pH 7.4). (C) Cryo-TEM image of MAA33 microgel in Tris buffer. (D) Microgel-induced hemolysis as a function of gel charge and concentration.

4.2 Model peptide interactions with MAA microgels (Paper I)

In Paper I, we studied the peptide loading and release of three molecular weights of the model peptide P-Lys onto three MAA microgels of different charge densities. The goal was to elucidate which factors influence peptide loading and release, including pH, ionic strength, gel charge density, peptide charge and length.

Peptide loading onto MAA33 microgels (*Figure 22A*) for P-Lys (1 kDa, 10 kDa and 150 kDa) induced microgel deswelling and was found to be promoted by shorter peptide length, demonstrating the importance of peptide length and charge, see *Figure 22B*. The shorter peptide has fewer charges per molecule and consequently more peptide molecules are required to neutralise the microgels, resulting in the difference in peptide loading between 1 kDa and 150 kDa P-Lys. The two shorter peptides can penetrate the polymer network and efficiently neutralise over 90% of the gel charges, whereas the longest 150 kDa peptide is too large and partially excluded from the cross-linked polymer network, achieving only 70% neutralisation, see Paper I. The size exclusion is further supported by the potential inversion observed in zeta potential measurements in Paper I. It is also in line with earlier reports of confocal microscopy observations for P-Lys loading onto acrylic acid-based microgels in the 100 µm regime, which clearly showed gel penetration for shorter P-Lys chains and shell formation for longer ones.[111]

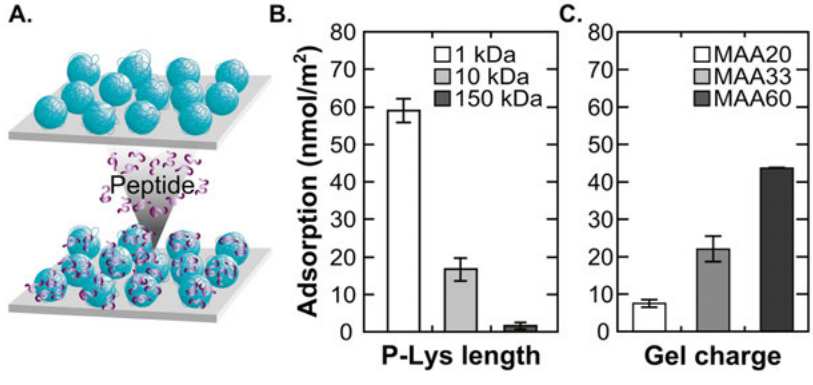

Figure 22. (A) Schematic of peptide binding to surface-bound microgels in ellipsometry, the mass change at the surface is modelled from the shift and amplitude change of elliptical light and presented for P-Lys in B and C. (B) Ellipsometry quantification of peptide loading of three different M_w of P-Lys (7.5 µM) onto surface-bound MAA33 microgels. (C) P-Lys (10 kDa, 7.5 µM) loading onto the three different charge densities of MAA microgels to highlight the importance of gel charge density, quantified by ellipsometry.

The importance of charge contrast between peptide and microgel was demonstrated again by loading 10 kDa P-Lys onto MAA microgels with different charge densities, see *Figure 22C*. The highest peptide binding was found for the gel with the highest charge, MAA60. The different charge densities of the synthesised microgel library can therefore be used to tune peptide loading.

Peptide release was studied as a function of peptide length, ionic strength and microgel charge density. It was found that peptide release was ineffective for the two longer P-Lys variants loaded onto MAA33 microgels, independent of

the ionic strength of the surrounding medium in the short (2 h) timeframe studied, see *Figure 23A*. The shortest P-Lys (1 kDa) displayed a modest ionic strength-dependent peptide release under the same conditions.

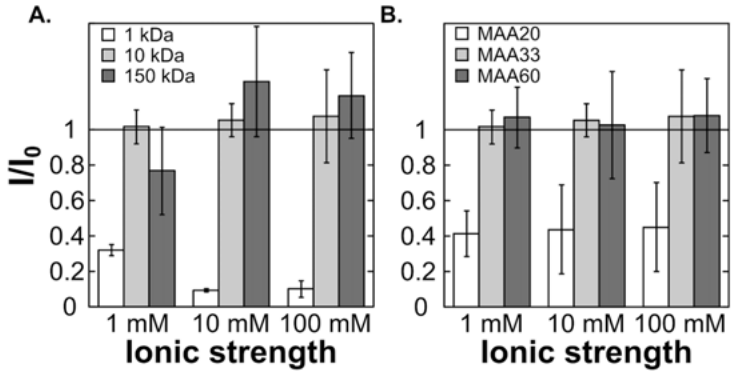

Figure 23. Confocal microscopy study of P-Lys release from microgels at different buffer ionic strengths for (A) different P-Lys lengths loaded onto MAA33 microgels and (B) different gel charge densities loaded with 10 kDa P-Lys. I/I_0 is the ratio between the fluorescence intensities from the gel-covered surfaces before (I_0) and after (I) peptide release through shaking in excess buffer for two hours.

Due to the high charge contrast between 10 kDa P-Lys and MAA microgels, the same difficulty in obtaining peptide release was encountered for MAA microgels of different charge densities at different ionic strengths. Only the lowest charged MAA20 microgel showed significant peptide release for the 10 kDa peptide, see *Figure 23B*. The release triggered at high electrolyte concentrations has been reported previously for acrylic acid-based microgels.[109]

Taken together, the results of Paper I demonstrate the importance of charge contrast between peptide and microgel for loading and release of the highly positively charged model peptide P-Lys. With this established, Papers II–IV used real therapeutic peptides to deepen the knowledge of AMP/microgel interactions, as well as consequences for membrane interactions and antimicrobial effects. The differences in molecular weight and charge between the three different P-Lys chains are dramatic: 1,000–150,000 g/mol and 30–1,000 in net charge. The differences in size and charge of the AMPs used in the following papers are much smaller, 2,500–4,500 g/mol and 3–7 in net charge, see *Table 1*. Consequently, the electrostatic interactions in AMP loading and release are expected to be weaker, potentially enabling peptide release under physiological conditions.

4.3 AMP interactions with MAA microgels and model membranes (Paper II)

In Paper II, peptide loading and release of two AMPs onto two MAA microgels of different charge densities were studied. In addition, their interactions with model membranes, as well as *in vitro* effects on bacteria, cells and enzymatic stability, were investigated.

4.3.1 AMP loading and release to/from MAA microgels

MAA26.5 and MAA60 microgels (*Table 2*) were evaluated as carriers for two selected linear AMPs, the shorter unstructured DPK-060 and the longer helix-adapting LL-37, see *Table 1* for specifications. Despite the fact that DPK-060 has twice the charge density of LL-37 and almost half the peptide length, LL-37 and DPK-060 still cover a much narrower range in size and charge than the model peptides used in Paper I. It was therefore expected that the peptide loading, as determined for surface-bound microgels in ellipsometry, would be more similar between these AMPs (see *Figure 24A*) than the dramatic difference found for different P-Lys lengths presented in Paper I (see *Figure 22B*). Both LL-37 and DPK-060 displayed high peptide loading onto MAA microgels of both charge densities studied (see *Figure 24A*), while the zeta potential indicated peptide incorporation into the gel core, Paper II.[50] Peptide binding increased somewhat with microgel charge density, see *Figure 24A*. In comparison, background binding to the underlying surface was found to be marginal. The peptide loading induced an α-helix conformation of LL-37, to similar degrees for both microgels, a behaviour reported when α-helix-forming peptides load onto oppositely charged microgels, see *Figure 24B*.[45,50,222,223]

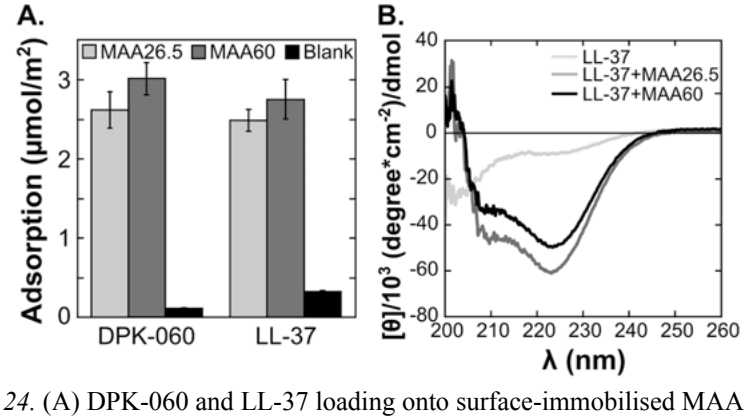

Figure 24. (A) DPK-060 and LL-37 loading onto surface-immobilised MAA microgels, as determined by ellipsometry. No significant differences between the charge densities of gels and only minor background adsorption of peptides were observed. (B) CD spectra in Tris buffer of LL-37 in free form and MAA microgel loaded. LL-37 adapted α-helix conformation upon microgel binding, compare with *Figure 14*.

Peptide release was studied using ellipsometry, see *Figure 25A*, and found to be triggered at physiological ionic strength, see *Figure 25B*. This is in line with the findings in Paper I, where the shortest P-Lys peptide (1 kDa), which is most similar to AMPs in size and charge, displayed peptide release induced at higher ionic strengths. It was found that up to 40% of bound LL-37 could be released over a time period of two hours, compared with up to 80% release for the shorter DPK-060. The increased peptide release from MAA microgel-loaded peptides at high ionic strength also gave rise to an increase in bacteria-mimicking DOPE/DOPG (3:1) liposome leakage, see *Figure 25C*. This effect was more pronounced for the lower charged MAA26.5 than for the higher charged MAA60 due to the stronger peptide binding to the latter. This increased liposome leakage at physiological ionic strength was observed while the free peptides at the same concentration suffered from partial inactivation due to electrostatic screening.

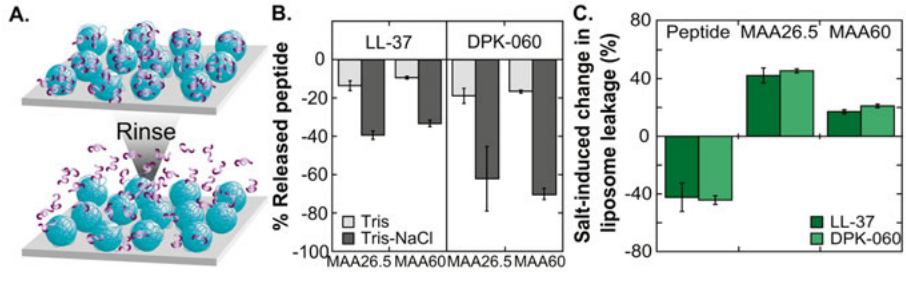

Figure 25. (A) Illustration of peptide release from surface-bound MAA microgels. (B) Peptide release as determined using ellipsometry by rinsing gel-covered surfaces with buffer at 1 mL/min for 2 h in Tris and Tris-NaCl (10 mM Tris, pH 7.4, 150 mM NaCl) buffer. (C) Differences in liposome leakage on bacteria modelling DOPE/DOPG (3:1) liposomes between Tris and Tris-NaCl buffer. A salt-induced increase in leakage was observed for MAA microgel-loaded peptide, whereas inactivation was observed for the free peptide upon increasing ionic strength.

4.3.2 AMP interactions with model membranes

As mentioned in Section 1.3, model membranes can be used both to screen for activity and for studying the mechanisms of membrane interaction for AMPs and AMP-loaded microgels, see *Figure 26A*. To verify that the negatively charged microgels had only minor interactions with negatively charged bacteria mimicking DOPE/DOPG (3:1) bilayers in ellipsometry, microgels were added in Tris buffer up to 1,000 ppm, see *Figure 26B*. As expected, no significant adsorption could be observed for either MAA26.5 or MAA60 microgels. When exposing the DOPE/DOPG bilayer to MAA microgels (10 ppm) loaded with LL-37 (0.3 µM) in Tris buffer, a minor increase in adsorption to the bilayer could be seen when compared with the free peptide, see *Figure 26C*. The mechanism of membrane interaction of LL-37 loaded MAA microgels was further studied in Paper III.

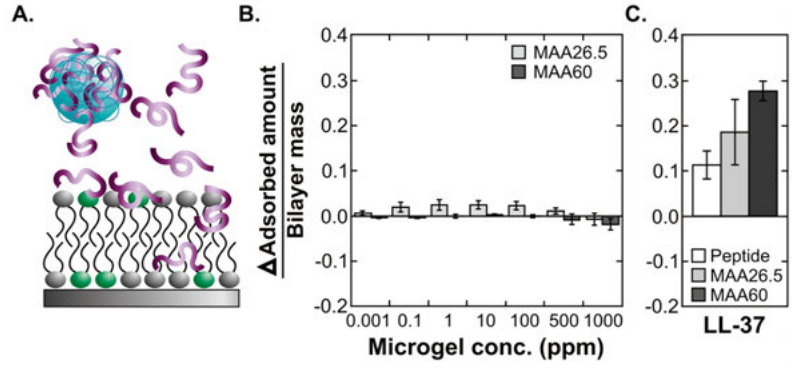

Figure 26. (A) Schematic illustration of peptide binding to a lipid bilayer in ellipsometry. (B) Ellipsometry data on MAA microgels and (C) DOPE/DOPG (3:1) bilayer interaction of LL-37 (0.3 μM) in free form and loaded onto MAA microgels (10 ppm). Microgels have minor binding to lipid bilayers (B) whereas LL-37 (C) affects the bilayer structure both in free form and when microgel-bound.

4.3.3 *In vitro* studies of AMPs

The antimicrobial activity of AMP-loaded MAA microgels was screened using MIC studies, *Table 3*. It was found that loading AMPs onto microgels maintained the antimicrobial activity for the peptide AP-114, increased the MIC for LL-37 and decreased the MIC significantly for DPK-060. The latter is a very interesting observation that needs further investigation, e.g., using neutron reflectometry. Speculatively, it could be due to combination effects between the AMP and the microgel, or simply that loading the peptide onto microgels minimises the inactivation due to salts and proteins in the experimental set-up with more effective peptide delivery to the bacteria as a result.

Table 3. MIC data for MAA26.5 and MAA60 loaded with DPK-060 and LL-37 on standard *E. coli*, *MRSA* and *PSA ATCC* (American Type Culture Collection) strains and a clinical isolate from the University Hospital of Angers, *PSA clin.*[*]

MIC (μM)	***E. coli***	***MRSA***	***PSA* ATCC**	***PSA* clin**
DPK-060	3.2	1.6	3.2	6.4
MAA26.5+DPK-060	1.6–3.2	0.8–1.6	0.8	0.8
MAA60+DPK-060	6.4	3.2	3.2	6.4
LL-37	3.6	1.8–3.6	1.8–3.6	1.8–3.6
MAA26.5+LL-37	> 7.1	> 7.1	7.1	> 7.1
MAA60+LL-37	> 7.1	> 7.1	> 7.1	> 7.1
AP-114	-	4	-	-
MAA26.5+AP-114	-	2–4	-	-

[*]Microgel without peptide displays no detectable antimicrobial effect up to at least 100 ppm.

As stated in the introduction, the sensitivity to proteolytic degradation is an obstacle in AMP therapeutics. DPK-060 is designed to withstand such

stresses, whereas LL-37 is one of the many AMPs susceptible to this kind of degradation. Formulating AMPs in gels has been shown to increase peptide stability. For example, loading the AMP LLKKK18 onto hyaluronic acid nanogels increased intracellular peptide stability.[82] The ratio of intact peptide was therefore determined for our microgel-peptide system before and after treatment with the bacterial enzyme *PSA elastase* for both free LL-37 and LL-37 loaded onto MAA26.5 and MAA60. The analysis before enzyme treatment verified that peptide loading onto MAA microgels does not degrade the peptide, a prerequisite for using MAA microgels for AMP-delivery. After treatment with *PSA elastase*, the majority of the free peptide was degraded. The same held true for LL-37 loaded onto MAA26.5, whereas the peptide remained intact when loaded onto MAA60, see *Figure 27A*. Hence, the higher charged gel is able to protect the peptide from enzymatic degradation and can therefore be a carrier candidate for sensitive peptides. The importance of gel charge density for proteolytic stabilisation of peptides has previously been highlighted for acrylic acid microgels, where P-Lys protection from Trypsin was observed only upon high peptide-microgel charge contrasts.[110] MAA26.5 was not able to protect LL-37 and might therefore be less suitable for sensitive peptides. Instead, it is suitable for chemically resistant peptides as DPK-060, with benefits such as decreased salt inactivation and improved peptide release.

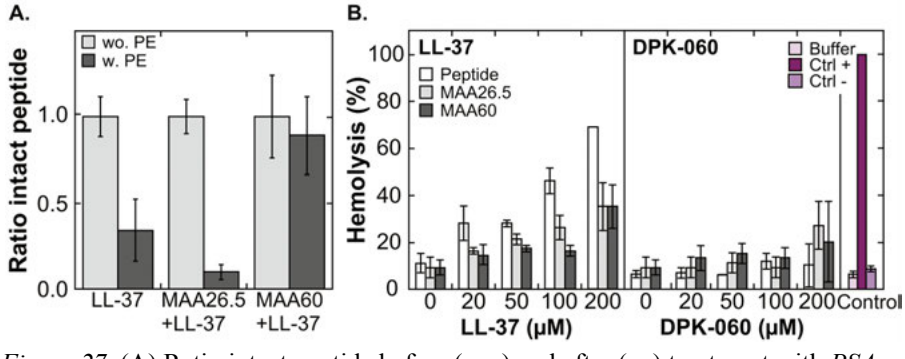

Figure 27. (A) Ratio intact peptide before (wo.) and after (w.) treatment with *PSA elastase* enzyme (PE) to free and MAA-microgel bound LL-37 (2 µg). The higher charged MAA60 microgel is able to protect the peptide from degradation, whereas the lower charged MAA26.5 microgel cannot. (B) Hemolysis experiments for empty (1,000 ppm) and peptide-loaded MAA microgels at the indicated concentrations.

Hemolysis experiments were also performed on MAA26.5 and MAA60 loaded with LL-37 and DPK-060, see *Figure 27B*. For DPK-060, which displays very low hemolysis of its own, hemolysis remained low after microgel binding. In contrast, free LL-37 displays higher toxicity to red blood cells. Formulating LL-37 in microgels decreased the recorded hemolysis significantly, especially for higher peptide concentrations. This is in line with an

earlier report where formulating novicidin in hyaluronic acid microgels reduced toxicity against HUVECs (human umbilical vein endothelial cells) and NIH-3T3 cells (mouse embryonic fibroblast cells) as compared with the free peptide.[81]

4.4 Membrane interactions of LL-37-loaded MAA microgels (Paper III)

In Paper III, NR was used to investigate, in greater depth, the mechanism of membrane interaction of MAA26.5 microgels (10 ppm) loaded with two different concentrations of LL-37 (0.3 µM, 5 µM). Deuterated DMPC/DMPG (3:1) lipids were used for the bilayer. Examples of reflectivity curves of bilayers before and after treatment with MAA26.5 and LL-37 samples in the d-contrast, together with modelled SLD profiles as a function of distance from the surface, are displayed in *Figure 28*.

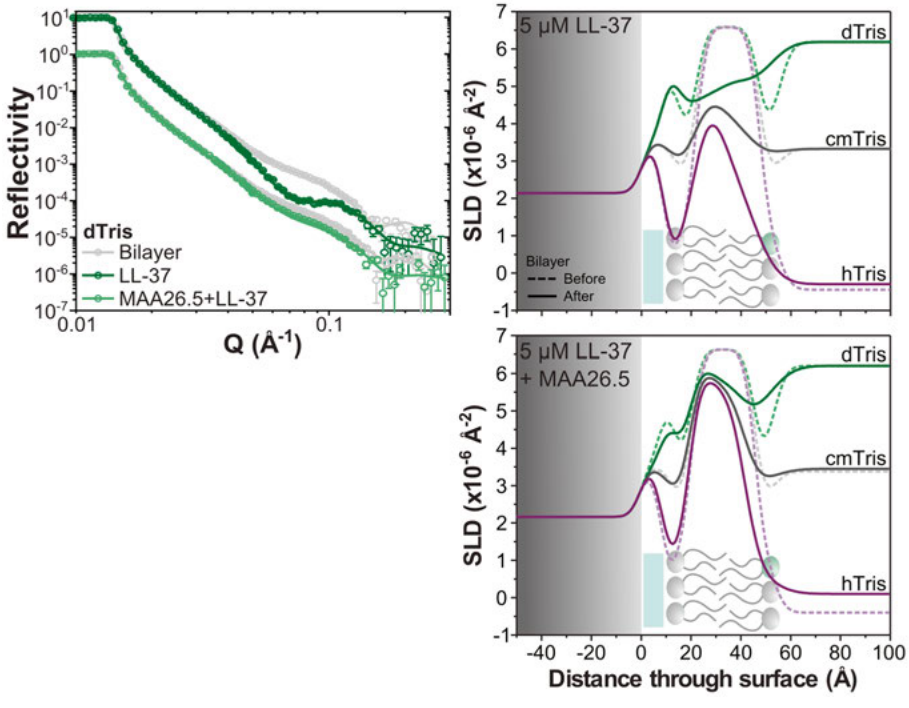

Figure 28. (Left) Neutron reflectivity profiles of the d-contrast and (right) modelled SLD profiles of deuterated DMPC/DMPG (3:1) bilayers treated with (top) free and (bottom) MAA26.5 bound 5 µM LL-37, respectively; broken lines before and solid lines after sample treatment. Defect formation is most pronounced for the free peptide. The grey box indicates the position of the silicon/silica interface.

The peptide interaction with the lipid bilayer was found to be concentration-dependent. At the lower LL-37 concentration (0.3 µM), the peptide primarily inserted into the outer lipid tail region of the bilayer without affecting the hydration, see *Figure 29A*. The peptide insertion also affected the thickness of the inner and outer tail regions, see *Figure 29B*. The findings for the lower peptide concentration indicate a two-step model where LL-37 primarily inserts in the outer leaflet and replaces lipids without any defect formation, in line with earlier findings.[224] At the higher peptide concentration (5 µM), major defects and hydration were observed in the bilayer due to removal of lipids, see *Figure 29C*.

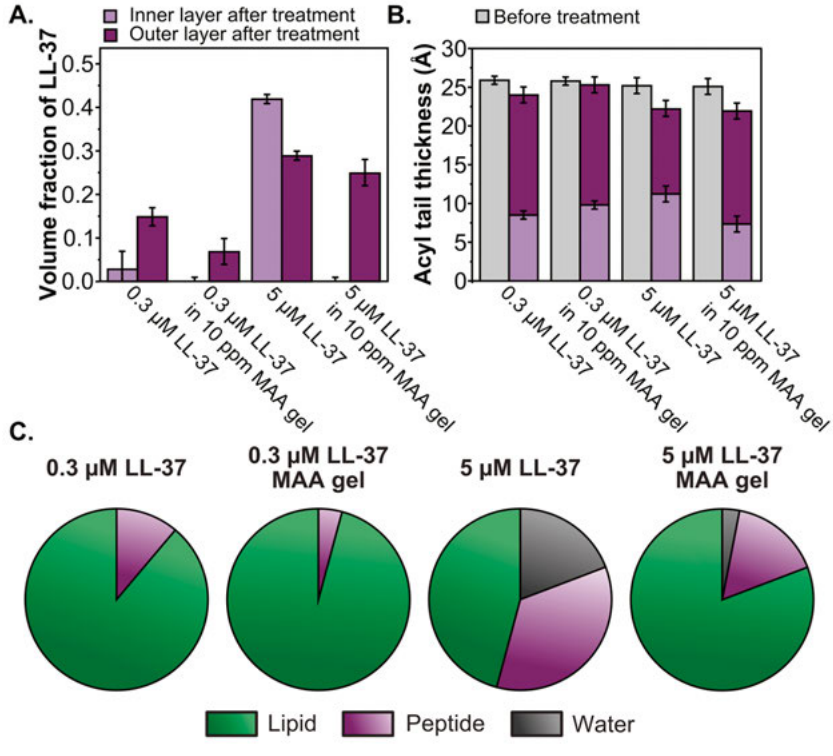

Figure 29. (A) Volume fraction of LL-37 in the bilayer after treatment with the indicated samples. The volume fraction of LL-37 in the bilayer increases with peptide concentration. MAA microgels decrease the amount of free peptide, hence also the volume fraction of LL-37 in the bilayer. (B) Initial acyl tail thickness of the deuterated DMPC/DMPG (3:1) bilayer compared with the thickness of the inner and outer lipid tail layer after treatment with the indicated samples. (C) Pie chart illustrations of the volume fraction of lipid, LL-37 and water in the tail region of the bilayer after treatment with the indicated samples.

There was no clear indication of microgels being present on top of the bilayer, which leads to the conclusion that the MAA microgels are passive peptide carriers that do not interfere with the peptide effect. However, due to slow

and/or incomplete peptide release, the presence of MAA microgels decreases the degree of bilayer defects, see *Figures 29* and *30*.

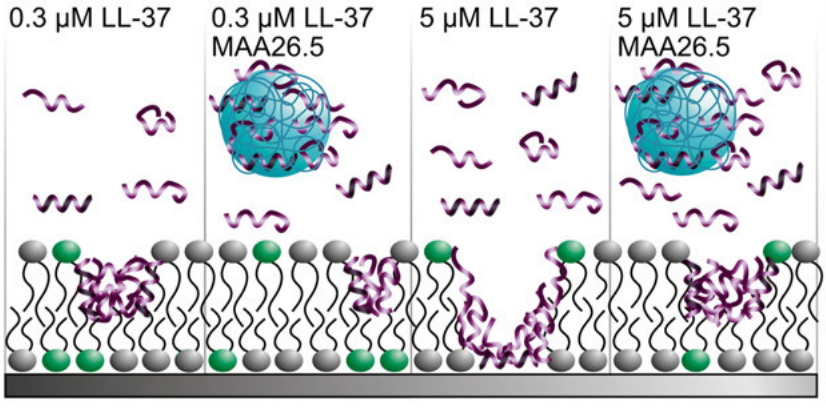

Figure 30. Schematic illustration of peptide interaction with the DMPC/DMPG (3:1) bilayer upon treatment with the indicated samples.

The mechanisms of membrane interactions of AMPs can vary with both the peptide studied and the lipid composition of the bilayer. For example, the hydrophilic peptide gH626-644 was found to prefer the hydrophilic head group region of DMPC and DMPG bilayers, while the hydrophobic gB632-650 peptide penetrated into the tail region.[225]

The bilayer interactions of LL-37 depends on the chain packing density of the lipids in the bilayer and the peptide prefers lipids with a low packing density, hence favouring PG over PC, PS and PE.[226] The mechanism of membrane interaction of LL-37 can therefore vary between model membranes and between bacterial strains, depending on their lipid composition, see *Figure 6*. Preference of LL-37 for the tail region of DMPC/DMPG bilayers was found in our study, and illustrates the importance of hydrophobic interactions. This is in line with findings in studies of LL-37 interaction with DOPC bilayers, where hydrophobic interactions were important for transmembrane pore formation,[224] as well as LL-37 helix insertion in DMPC and DMPC/DMPG lipid bilayers.[49,227]

In conclusion, when loading LL-37 onto MAA microgels, the antimicrobial unit is primarily the released peptide. The mechanism of membrane interaction with a DMPC/DMPG bilayer is peptide concentration-dependent, with peptide insertion in the outer lipid tail region at low concentration and transmembrane defect formation and lipid removal at high peptide concentrations.

4.5 Effect of PEGylation on AMP loading and release (Paper IV)

PEGylation of drugs, nanoparticles and AMPs is known to increase performance through increased circulation times, decreased aggregation and toxicity. However, PEGylation may not completely protect peptides from proteolytic degradation. As presented in Paper II, MAA microgels can offer improved protection, making a study of the interactions between PEGylated AMPs and MAA microgels interesting. In Paper IV, the effect of peptide PEGylation on the interaction with MAA microgels was studied using the broad-spectrum AMP KYE-28; peptide specifications can be found in Section 1.1 and in *Table 1*. Both the peptide/microgel interactions and the effect of PEGylation site were of interest.

KYE-28 was used either in its native form or with 48 PEG units at the C-terminal or at the N-terminal or 24 PEG units at each site, see *Figure 31A*. It was found that non-PEGylated smaller KYE-28 had a higher peptide loading onto MAA60 microgels as compared with the larger PEGylated variants, see *Figure 31B*. PEGylation suppressed peptide binding, while the PEGylation site had no significant influence on peptide loading. In contrast, the length of the PEG unit can be of importance for peptide loading and release to/from anionic microgels, in line with earlier reports, where increasing PEGylation length suppressed KYE-28 interactions with anionic model membranes.[38] PEGylation site affected peptide conformation in CD. KYE-28 is an α-helix-forming peptide, and the α-helix formation is promoted by PEGylation at the N-terminal of the peptide (**PEG48**KYE-28 > **PEG24**KYE-28**PEG24**) (see *Figure 31C*), indicating that PEGylation site can be of importance for factors not studied here, such as peptide stability[44] and membrane interactions.[228]

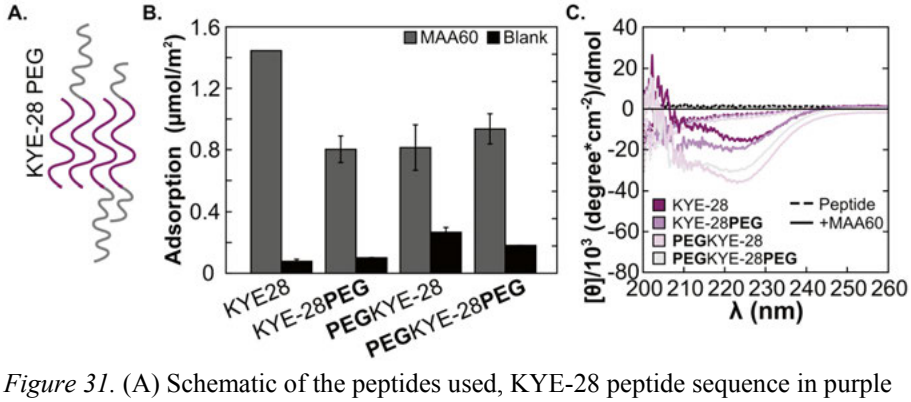

Figure 31. (A) Schematic of the peptides used, KYE-28 peptide sequence in purple and PEG in grey. (B) Peptide loading onto MAA60 microgels measured using ellipsometry. (C) CD spectra of MAA60 microgel-loaded KYE-28 and its PEGylated variants. α-helix conformation is induced upon peptide loading and most pronounced upon PEGylation at the N-terminal.

Peptide-microgel interactions were studied using NMR spectroscopy to determine peptide conformation of KYE-28 and its PEGylated variants when loaded onto MAA60 microgels. Various 2D NMR techniques such as TOCSY, NOESY, *tr*NOESY, and 1D STD experiments were used. *tr*NOESY showed that both electrostatic interactions between peptide and gel and hydrophobic interactions within the peptide were important for the peptide structure in the gel (see *Figure 32A*). This is in line with earlier findings for the AMP EFK-17.[83] A conformation could be obtained for microgel-bound KYE-28**PEG** (see *Figure 32B*), showing the hydrophobic interactions giving rise to the cross-peaks in *Figure 32A* and that KYE-28 partially adapts a helix conformation, as indicated by the CD spectra in *Figure 31C*. For KYE-28 and the other two PEGylated variants, too few medium- and long-range NOEs were obtained to calculate a distinct conformation due to strong microgel-binding for KYE-28 and weak interactions for the other PEGylated variants.

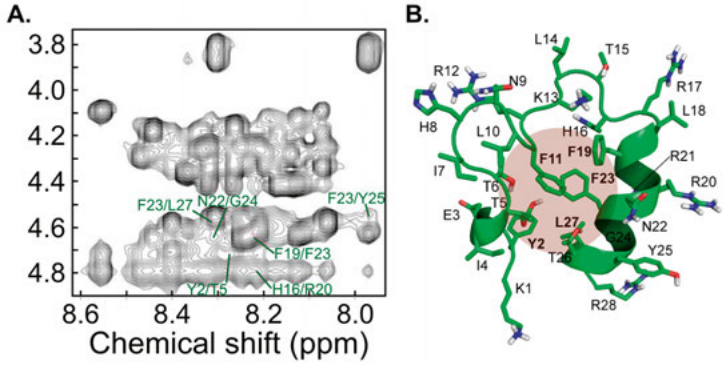

Figure 32. (A) The medium-range NOEs from the 2D-*tr*NOESY spectra of KYE-28**PEG** after MAA60 microgel addition. (B) Structure of KYE-28**PEG** upon binding to MAA60 microgels, as determined by NMR spectroscopy.

Peptide release was found to be induced at physiological ionic strength, in agreement with the findings in Papers I and II. The release was found to be promoted by peptide PEGylation regardless of PEGylation site, see *Figure 33*.

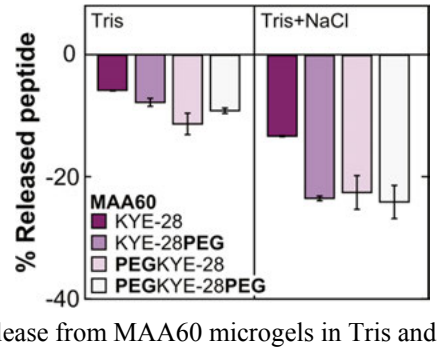

Figure 33. Peptide release from MAA60 microgels in Tris and Tris-NaCl buffer. Peptide release is promoted by buffer ionic strength and peptide PEGylation.

4.6 AMP interaction with DNGs and model membranes (Paper V)

In Paper V, the AMP loading and release to/from degradable DNGs were studied in relation to the charge density, cross-linker density and degradation of the gel network. The consequences for hemolysis and antimicrobial effects were also approached.

4.6.1 AMP loading and release to/from DNGs

A library of degradable DNGs was developed and synthesised with the aim to obtain a biocompatible and degradable material.[108,121] The suggested network architecture was briefly described in Section 1.2.3 and illustrated in *Figure 5*. Three different DNGs were used in Paper V: DNG1–3, all with different charge and cross-linker densities (specifications in Section 1.2.3).

Peptide binding was quantified using BCA as described in Section 3.2.3 and found to be dependent on gel charge density for the shorter DPK-060 peptide, and independent thereof for the longer LL-37 peptide, see *Figure 34A*. The shorter peptide was able to penetrate into the charged cross-linked cores, whereas results on peptide binding, conformation, and susceptibility to proteolytic degradation all indicated that the longer LL-37 peptide was unable to penetrate the cores, instead residing primarily in the PEG corona. Overall, the peptide binding was lower than that of MAA microgels in Papers I–IV. This is due to weaker charge and higher cross-linker density of the DNGs, excluding longer peptides for the charged cores. Despite the tighter network, the gel charges can be used as peptide-binding sites, as demonstrated by the 40–80% neutralisation in *Figure 34B*. This can be compared with the 70% LLKKK18 binding[82] and 15–71% novicidin binding[81] to hyaluronic acid microgels. The peptide release was found to be triggered at physiological ionic strength, in line with the results in Papers I, II and IV. This demonstrates the importance of electrostatic screening as a driving force for peptide release in charged carrier systems.

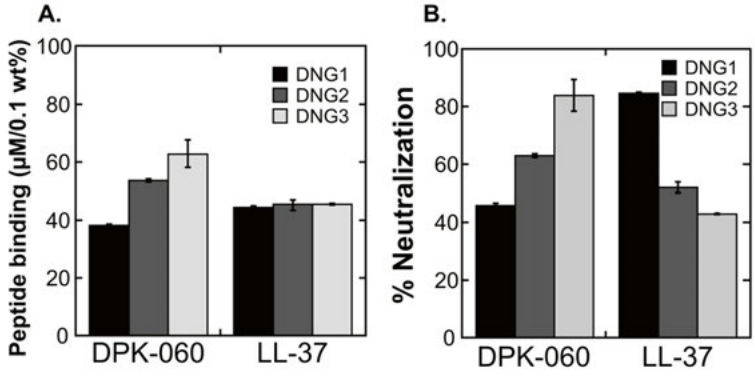

Figure 34. (A) Peptide loading to DNGs (1,000 ppm) determined by BCA analysis as described in 3.2.[180] (B) Gel neutralisation resulting from peptide binding in (A).

4.6.2 Membrane interactions of AMPs loaded to DNGs

An interesting aspect of a degradable system is how the degradability influences peptide release and effect. The DNG degradation could be monitored using the intensity of the ester peak in FTIR spectroscopy. The ratio of intact ester bonds was found to reach a plateau after 10 days, as exemplified for DNG1 in *Figure 35A*. Interestingly, the leakage of bacteria modelling DOPE/DOPG (3:1) liposomes was decoupled from the degradation of the nanogel network, as the liposome leakage changed dramatically over the initial 6 hours and then reached a plateau, see *Figure 35B*. This decoupled mechanism indicates a rapid onset of the peptide release, which often is desired when treating acute infections. When longer release times are required, e.g., to avoid infections at implant sites, either a re-design of the DNGs is necessary or other drug carrier systems with longer release times should be used.[81]

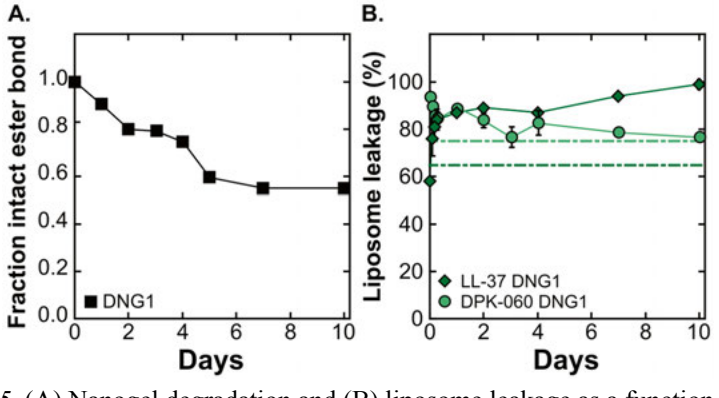

Figure 35. (A) Nanogel degradation and (B) liposome leakage as a function of degradation time for DNG1 (10 ppm, 0.3 µM LL-37). Degradation was monitored through the decline of the ester peak at 1,736 cm^{-1} in FTIR spectroscopy.

To get an indication of the biocompatibility of the DNGs, hemolysis experiments were performed on DNGs, both empty and loaded with LL-37 and DPK-060, see *Figure 36*. Only minor lysis of red blood cells was detected for each of the samples.

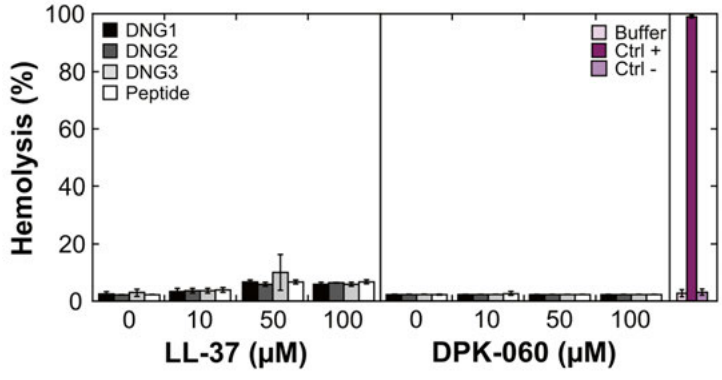

Figure 36. Lysis of red blood cells (hemolysis) caused by free or DNG-loaded AMPs, either LL-37 (left) or DPK-060 (right), at the indicated concentrations.

In summary, the DNGs offer low hemolysis, efficient peptide binding and a fast peptide release, decoupled from the network degradation. The benefit of degradability is avoiding accumulation-related side effects rather than to function as a trigger for peptide release. For some DNG/peptide combinations, the peptide seems to reside in the PEG corona due to size exclusion from the highly cross-linked anionic cores. Smaller peptides as DPK-060[50] and GNU6-7 (1,888 g/mol)[229] might therefore be the preferred cargo for DNGs, rather than longer AMPs, such as LL-37. Membrane binding and destabilisation of peptide-loaded DNGs are improved or comparable to that of the free peptides, in line with the preserved antimicrobial effect after AMP incorporation in DNGs.

5. Conclusion

The focus of this thesis was on systematic evaluation of factors affecting peptide and membrane interactions when polymer nanomaterials were used as carriers for peptides. Two different gel libraries have been evaluated: methacrylic acid-based MAA microgels and degradable DNGs. Factors relating to the carrier material (composition, degradability, charge and cross-linker density), peptide properties (sequence, charge, size, PEGylation and secondary structure) and the surrounding media (ionic strength and pH) were addressed, to better understand what aspects are important when developing a carrier system for a peptide.

It was found that the electrostatic contrast between MAA microgels and peptides is essential for peptide loading and release, see Paper I. For the loading of P-Lys onto MAA microgels, a high gel charge promoted peptide loading, but suppressed peptide release. The importance of gel mesh and peptide size was shown, as the shortest P-Lys could penetrate the gel, whereas the longest P-Lys chain was excluded from the gel network. Screening the electrostatic contrast between gel and peptide by increasing the ionic strength led to decreased peptide loading and increased peptide release, but primarily for the shortest peptide investigated.

Similar effects were observed for the loading of the AMPs LL-37, DPK-060, KYE-28 and its PEGylated variants, Papers II and IV. The unmodified peptides all displayed promising peptide loading and core incorporation, whereas all the large PEGylated KYE-28 were restricted to the microgel palisade due to size exclusion from the microgel network, independent of PEGylation site.

Detailed structural studies of KYE-28PEG showed that the electrostatic interactions with the microgels were important for peptide loading, but the interactions between hydrophobic amino acids should not be underestimated as a factor for peptide stabilisation or peptide loading, see Paper IV.

The importance of gel charge for peptide stabilisation was demonstrated, as the MAA microgel with highest charge could protect LL-37 from proteolytic degradation whereas gels with lower charge density could not, see Paper II.

Peptide release was found to be triggered at physiological ionic strength for all three AMPs above and the PEGylated variants of KYE-28 (Papers II and IV), in line with the results obtained for P-Lys.

The interaction with model lipid bilayers at low (10 mM) ionic strength is negligible for AMP-loaded MAA microgels. As the ionic strength is increased to physiologically relevant 150 mM, peptide release and resulting membrane interaction of free peptide are triggered, see Paper II. Therefore, membrane interactions for LL-37 loaded MAA microgels are primarily mediated by released peptide, see Paper III. When interacting with a DMPC/DMPG bilayer, the peptide resides in the tail region of the bilayer. At low peptide concentrations, the effect on the outer leaflet is most pronounced, while defects on the inner leaflet were observed with increasing peptide concentration. The antimicrobial effects of peptide-loaded MAA microgels are promoted by decreasing gel and peptide charge, factors that again facilitate peptide release, see Paper II.

For the degradable DNGs with tightly bound microgel cores, core incorporation was observed for DPK-060 (2.5 kDa), but not for LL-37 (4.5 kDa), indicating the importance of sufficient matrix mesh size, see Paper V. Peptide release from DNGs was found to be independent of gel network degradation.

The liposome leakage observed for free LL-37 is preserved upon peptide incorporation/binding to DNGs. In comparison, DPK-060 incorporation somewhat decreases liposome leakage, likely due to incomplete peptide release in the timeframe studied. In VCA analyses, the antimicrobial effects of DNG bound peptides mirror those of the free peptides, illustrating that network degradation and peptide release are decoupled processes, see Paper V.

In order to obtain an optimal delivery system, it is important to find the right carrier for the AMP in question. Variations in peptide length, hydrophobicity and charge can alter the behaviour of the system. MAA microgels and DNGs both display properties that could make them interesting as carriers for AMPs, including low hemolysis, protection of the peptide against infection-related proteolysis, and maintained or even improved *in vitro* antimicrobial effect.

Overall, this thesis has contributed to understanding of the interactions between polymer nanoparticles and AMPs, including factors affecting peptide loading, protection and release. In addition, AMP interactions with model membranes, red blood cells and several bacterial strains have been investigated, to evaluate peptide effect after incorporation in nanoparticles and to understand the mechanisms of membrane interactions.

6. Future perspective

The development of drug carrier and delivery systems for bio-macromolecular drugs is an important and interesting field. Key factors affecting a peptide carrier system were investigated in this work, with promising results. Future work would include moving closer to the actual intended product, a commercially available peptide formulation using micro- and nanogels.

One challenge ahead is to elucidate what risks are associated with the use of these carrier nanomaterials *in vivo* in terms of degradation, accumulation, immunoresponse and aggregation.

The pharmacodynamics of these peptide carriers are interesting, as many of the AMPs are multifunctional, with antimicrobial, immunomodulatory and anticancer effects, to name a few. For example, a combination of immunomodulation and antimicrobial effects is very interesting in biomaterial coatings, to decrease the risks for infection and inflammation. Surface-immobilised microgels can be a way of introducing multifunctional peptides at implant sites.

Pharmacokinetic aspects are important, since many antimicrobial peptides are sensitive to enzymatic activity causing fast degradation and clearance. As shown in this thesis, the right peptide carrier can protect the peptide from such attacks. In relation to this, it is important to understand how the protection affects both the peptide concentration *in vivo* and the drug half-life.

Minimising AMP use decreases the rate of resistance development and can be achieved through local delivery, triggered release and combination therapies. Local delivery minimises the AMP dose required; some microgels might be suitable for topical formulations, while others are better for pulmonary routes. Introducing antibodies as microgel triggers instead of carboxylic acids induces peptide release only upon infection and minimises unnecessary AMP exposure. Using conventional antibiotics in combination with AMPs can improve efficiency, and shorten therapy duration and the cost of goods.

AMPs are not our ultimate weapon against bacterial infections, but rather one tool in a vast and growing toolbox. Other alternatives are antibacterial polymers and vaccines, to name a few. Due to resistance development, we will need to continually explore alternative routes to treat bacterial infections.

7. Populärvetenskaplig sammanfattning

Antibiotikaresistens är ett växande problem i världen. Allt fler bakteriestammar utvecklar resistans mot fler av våra tillgängliga antibiotika vilket har lett till att sjukdomar vi tidigare enkelt behandlat blir allt svårare att bota. Samtidigt har lanseringen av nya antibiotika stannat av de senaste decennierna. För att vi långsiktigt ska kunna behandla till och med vanliga bakteriesjukdomar måste utvecklingen av nya behandlingsmetoder ta fart.

Ett alternativt medel är antimikrobiella peptider (AMP). AMPar är små positivt laddade proteiner som är en del av det naturliga immunförsvaret i alla levande organismer. AMPar har utvecklats parallellt med bakterier under lång tid utan betydande resistensutveckling. Klassiska antibiotika verkar vanligen på celldelningen hos bakterier. AMPar agerar istället på flera vitala funktioner samtidigt, dock främst genom att skapa porer i bakteriernas cellväggar, vilket får bakterierna att lösas upp och dö.

Det finns många problem med AMPar: de kan vara toxiska för mänskliga celler, bli inaktiverade av salthalten och proteiner i kroppen eller brytas ner av kroppens enzymer. För att skydda AMParna mot dessa kemiska och enzymatiska hinder kan man använda sig av läkemedelsbärare. Mikro- och nanogeler har väckt stort intresse som läkemedelsbärare för peptider och proteiner. Dessa geler består av polymera fibrer och påminner om garnnystan som kan expandera eller komprimeras. Denna förändring kan aktiveras genom en lång rad olika stimuli beroende på hur gelen är designad, vilket gör att peptidinladdning och frisättning kan utlösas på ackord. Stimuli kan vara ökad salthalt i kroppen, förändrat pH i infekterad vävnad, temperaturförändringar osv.

I den här avhandlingen utvärderas två olika typer av responsiva geler som bärare för AMPar, icke-degraderbara MAA mikrogeler och degraderbara dendritiska nanogeler (DNG). Gelerna är 100-200 nm i diameter, så små att ögat inte kan urskilja dem. I avhandlingen diskuteras de många faktorer som påverkar AMP inladdning, frisättning, skydd och effekt, *Figur 1*. Bland de undersökta faktorerna kan nämnas gelernas struktur och laddning, peptidernas längd, form och laddning samt omgivningens pH och salthalt.

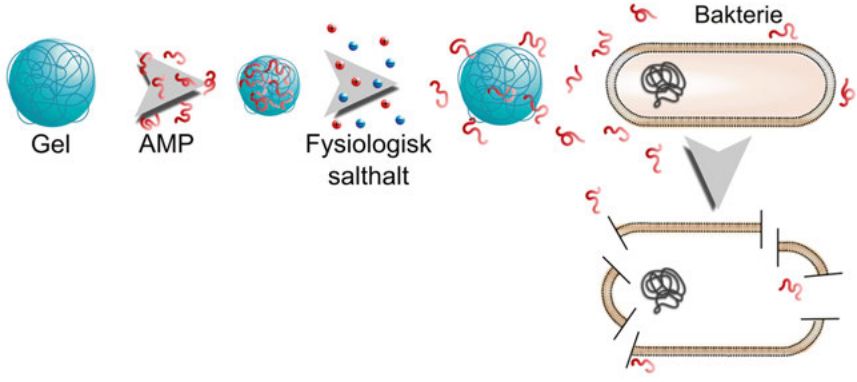

Figur 1. Schematisk illustration av (från vänster) en gel som laddas med AMP; frisättning av AMP triggad av fysiologisk salthalt; frisatt AMP interagerar med bakteriens membran och skapar porer i det, vilket leder till bakteriens död.

MAA mikrogelerna är negativt laddade vid fysiologiskt pH. Inladdning av positivt laddade AMPar sker genom elektrostatisk attraktion, medan frisättning utlöses vid fysiologisk salthalt. AMParna binder till kärnan i MAA mikrogeler vilket skyddar mot de ovan nämnda problemen med inaktivering och nedbrytning samtidigt som toxiciteten minskar jämfört med fri peptid. Gelens laddning styr AMP inladdning och frisättning. Högre laddning ger starkare och effektivare inladdning, men sämre frisättning av AMPar. Minskad gelladdning ger bättre frisättning, men lägre inladdning och sämre skydd av AMPen mot proteolytisk nedbrytning. Interaktioner med modellbakteriemembran och den antimikrobiella effekten av AMParna bevarades efter inladdning i mikrogeler. Studier visade att den antimikrobiella enheten i systemet främst är frisatt peptid, och att gelen är en passiv läkemedelsbärare. Ett passivt system är lättare att motivera för myndigheter än ett aktivt system som påverkar effekten.

DNG är intressanta som bärare för AMPar då de är nedbrytbara i kroppen och löses upp efter behandling. Det gör att det inte blir några restprodukter och material kvar. Studien indikerade att DNG är mycket biokompatibla med en låg toxicitet. Gelerna kunde ladda in AMPar och frisätta dem genom ökad salthalt, precis som för MAA mikrogelerna som nämndes ovan. Peptidfrisättningen var snabb och helt oberoende av gelnedbrytningen. Den antimikrobiella effekten på *E. coli* bakterier var bevarad jämfört med fri peptid.

Sammantaget har båda studerade gelerna visat lovande egenskaper som bärare för antimikrobiella peptider. Vidare studier kan visa om de är möjliga att använda i riktiga läkemedelsformuleringar.

8. Acknowledgements

This work was conducted at the *Department of Pharmacy*, Uppsala university, and was supported by the *EU Seventh framework programme (FORMAMP)* and the *Swedish research council*. Neutron beam time and grants were gratefully received from The *Institut Laue-Langevin* (France) and *ISIS Neutron and Muon Source* (UK). Highly appreciated travel grants were received from *Apotekarsocieteten* and *Smålands nation*.

To my supervisor, *Martin Malmsten*, for taking me on as a PhD student, allowing me to find my own way and putting together an environment of wonderful people around me, making the laboratory a great place to be. And of course for your insanely quick email replies. To my co-supervisor *Per Hansson,* for helping me solve my biggest head scratcher: aggregating gels at homeopathic peptide concentrations. To my co-supervisor and FORMAMP coordinator Helena Bysell for your good advice and nice lunches when I needed them the most.

To all *former and present staff* at the Department of Pharmacy, for the positive and inclusive working environment!

To Professor *Brian Saunders* and Dr *Jane Bramhill* at Manchester University, for expertise and supervision during microgel synthesis and characterisation. To *Elisa, Tomas* and *Jonny* for great collaborations.

I'm grateful to my FORMAMP colleagues, collaborators and co-authors for fruitful discussions, feedback and all the good times we've spent together both at and outside meetings and laboratories! Special thanks to *Oliver, Mina, Lukas, Anita* and *Katharina* for invaluable collaborations.

Claes, for being the best first office mate ever where "vet du vad som gör mig jävligt förbannad" always started hours of discussions. To *Rosita*, my third office-mate, for clever input, nice chats and for making me productive! Till *Lotta,* för att du är du, och för att du alltid spred den fantastiska "Lotta"-känslan på labb. To *Kate*, for introducing me to neutrons and Dead of Winter and for forever changing my opinion on speedbumps and berets. To *Sara,* for your energy, enthusiasm and for Disney Fridays. To *Shalini*, *Ronja* and *Yanling,* for the great atmosphere at work. To present group members: *Agnes, Julia,*

Marcus, Sana, Vahid, Franz, Yassir, Sean and *Anna,* for the nice collaborative spirit you have created in our laboratory and for your support these last couple of months.

To *Lina*, for your different and helpful perspectives and ideas regarding our research and all the invaluable whiteboard sessions, but most of all for the support, fun times and adventures during our PhD years.

To former and present members of the *AGHG group*, for being my safe haven on the stormy sea of research and for saving me every time I needed organic chemistry equipment or a nice night out. Especially to *Hao,* for being a fantastic friend, but also for sharing my interest in fine aroma variations in wine and tea.

To *Hanna* and *Jenny* for 10+ years of fantastic support and encouragement. Hard times are best survived with great company and laughter. Thanks to *Sandra*, for putting up with me all these years, despite my culinary ideas, photo projects on cold winter nights and terrible songs about guitars. Friendship without limits is a rare find. To *Elias* and *Sandra* for breaking Knally. To my *IUPAK*-related friends, *Malin, Hilde, Sarah, Mathias, Nils, Andreas, Petter,* and everyone else.

To my family: *Tomas, Karin* and *Johanna,* for cheering me on from the side lines. Till *mamma*, för ditt aldrig vikande stöd, för ditt oändliga tålamod, och för att du hade is i magen, även när journalisten och fotografen skulle bli kemist. Så här elva år senare kan vi ju se att det gick OK. Till *Magnus,* för att du försiktigt och utan frågor tog dig an mig. Tack vare dig är jag en av få som har lyckan att ha haft två fantastiska fadersgestalter i mitt liv. Till min partner i allt, *Micke*, för att du är det smartaste bollplank och den bästa klippan som finns. Som härifrån och till månen kan inte börja att beskriva vad du betytt för den här avhandlingen och vad du betyder för mig. Till *Tanja*, för att du är coolare än glass, tuffare än tåget och sötare än julmust!

To everyone who is trying to find their name and has realised that I have forgotten to write to you. Here comes a big THANK YOU from me to you! I'm so sorry I've forgotten to add you more specifically, it's not from a lack of gratitude, but rather due to the strange ways of a stressed-out mind. I hope you can forgive me!

Thank you!
Randi Nordström
Uppsala, October 2019

9. References

(1) World Health Organization. *Antimicrobial resistance : global report on surveillance*; **2014**.
(2) Food and Drug Administration. *CFR Annual Print Title 21 Food and Drugs*; **2018**.
(3) Cassini, A.; Högberg, L. D.; Plachouras, D.; Quattrocchi, A.; Hoxha, A.; Simonsen, G. S.; Colomb-Cotinat, M.; Kretzschmar, M. E.; Devleesschauwer, B.; Cecchini, M.; Ouakrim, D. A.; Oliveira, T. C.; Struelens, M. J.; Suetens, C.; Monnet, D. L. *Lancet. Infect. Dis.* **2019**, *19* (1), 56–66.
(4) Hofer, U. *Nat. Rev. Microbiol.* **2019**, *17* (1), 3–3.
(5) Public Health Agency of Sweden. *Future costs of antibiotic resistance Final reporting of Government commission on direct and indirect costs and consequences of antibiotic resistance in Swedish health care*; Solna, 2018.
(6) Fleming, A. *Br. J. Exp. Pathol.* **1929**, *10* (3), 226–236.
(7) Bebbington, C.; Yarranton, G. *Curr. Opin. Biotechnol.* **2008**, *19* (6), 613–619.
(8) Whitney, C. G.; Farley, M. M.; Hadler, J.; Harrison, L. H.; Bennett, N. M.; Lynfield, R.; Reingold, A.; Cieslak, P. R.; Pilishvili, T.; Jackson, D.; Facklam, R. R.; Jorgensen, J. H.; Schuchat, A. *N. Engl. J. Med.* **2003**, *348* (18), 1737–1746.
(9) Zasloff, M. *Nature* **2002**, *415* (6870), 389–395.
(10) Czaplewski, L.; Bax, R.; Clokie, M.; Dawson, M.; Fairhead, H.; Fischetti, V. A.; Foster, S.; Gilmore, B. F.; Hancock, R. E. W.; Harper, D.; Henderson, I. R.; Hilpert, K.; Jones, B. V; Kadioglu, A.; Knowles, D.; Ólafsdóttir, S.; Payne, D.; Projan, S.; Shaunak, S.; Silverman, J.; Thomas, C. M.; Trust, T. J.; Warn, P.; Rex, J. H. *Lancet. Infect. Dis.* **2016**, *16* (2), 239–251.
(11) Ghosh, C.; Sarkar, P.; Issa, R.; Haldar, J. *Trends Microbiol.* **2019**, *27* (4), 323–338.
(12) Hancock, R. E. W.; Sahl, H.-G. *Nat. Biotechnol.* **2006**, *24* (12), 1551–1557.
(13) Tenland, E.; Krishnan, N.; Rönnholm, A.; Kalsum, S.; Puthia, M.; Mörgelin, M.; Davoudi, M.; Otrocka, M.; Alaridah, N.; Glegola-Madejska, I.; Sturegård, E.; Schmidtchen, A.; Lerm, M.; Robertson, B. D.; Godaly, G. *Tuberculosis* **2018**, *113*, 231–238.
(14) Peschel, A.; Sahl, H.-G. *Nat. Rev. Microbiol.* **2006**, *4* (7), 529–536.
(15) Andersson, D. I.; Hughes, D.; Kubicek-Sutherland, J. Z. *Drug Resist. Updat.* **2016**, *26*, 43–57.
(16) Epand, R. M.; Vogel, H. J. *Biochim. Biophys. Acta - Biomembr.* **1999**, *1462* (1–2), 11–28.
(17) Shai, Y. *Biopolymers* **2002**, *66* (4), 236–248.
(18) Bechinger, B.; Gorr, S. U. *Journal of Dental Research*. International Association for Dental Research **2017**, 254–260.
(19) Joo, H. S.; Otto, M. *Biochimica et Biophysica Acta - Biomembranes*. November **2015**, 3055–3061.

(20) Joo, H. S.; Fu, C. I.; Otto, M. *Philos. Trans. R. Soc. B Biol. Sci.* **2016**, *371* (1695), 20150292.
(21) Nizet, V. *Curr. Issues Mol. Biol.* **2006**, *8* (1), 11–26.
(22) Farnoud, A. M.; Toledo, A. M.; Konopka, J. B.; Del Poeta, M.; London, E. *Curr. Top. Membr.* **2015**, *75*, 233–268.
(23) Wang, J. H.; Liu, X. H.; Mao, R. Y. *RCSB PDB*.
(24) Datta, A.; Bhattacharyya, D.; Singh, S.; Ghosh, A.; Schmidtchen, A.; Malmsten, M.; Bhunia, A. *J. Biol. Chem.* **2016**, *291*, 13301–13317.
(25) Wang, G. *J.Biol.Chem.* **2008**, *283*, 32637–32643.
(26) Berman, H. M.; Westbrook, J.; Zukang, F.; Gilliland, G.; Bhat, T. N.; Weissig, H.; Shindyalov, I. N.; Bourne, P. E. *Nucleic Acids Res.* **2000**, *28* (1), 235–242.
(27) Kyte, J.; Doolittle, R. F. *J. Mol. Biol.* **1982**, *157* (1), 105–132.
(28) Nyström, L.; Nordström, R.; Bramhill, J.; Saunders, B. R.; Álvarez-Asencio, R.; Rutland, M. W.; Malmsten, M. *Biomacromolecules* **2016**, *17* (2), 669–678.
(29) Mygind, P. H.; Fischer, R. L.; Schnorr, K. M.; Hansen, M. T.; Sönksen, C. P.; Ludvigsen, S.; Raventós, D.; Buskov, S.; Christensen, B.; De Maria, L.; Taboureau, O.; Yaver, D.; Elvig-Jørgensen, S. G.; Sørensen, M. V.; Christensen, B. E.; Kjærulff, S.; Frimodt-Moller, N.; Lehrer, R. I.; Zasloff, M.; Kristensen, H.-H. *Nature* **2005**, *437* (7061), 975–980.
(30) Brinch, K. S.; Tulkens, P. M.; Van Bambeke, F.; Frimodt-Moller, N.; Hoiby, N.; Kristensen, H.-H. *J. Antimicrob. Chemother.* **2010**, *65* (8), 1720–1724.
(31) Schneider, T.; Kruse, T.; Wimmer, R.; Wiedemann, I.; Sass, V.; Pag, U.; Jansen, A.; Nielsen, A. K.; Mygind, P. H.; Raventos, D. S.; Neve, S.; Ravn, B.; Bonvin, A. M. J. J.; De Maria, L.; Andersen, A. S.; Gammelgaard, L. K.; Sahl, H.-G.; Kristensen, H.-H. *Science.* **2010**, *328* (5982), 1168–1172.
(32) Xiong, Y. Q.; Hady, W. A.; Deslandes, A.; Rey, A.; Fraisse, L.; Kristensen, H.-H.; Yeaman, M. R.; Bayer, A. S. *Antimicrob. Agents Chemother.* **2011**, *55* (11), 5325–5330.
(33) Schmidtchen, A.; Pasupuleti, M.; Mörgelin, M.; Davoudi, M.; Alenfall, J.; Chalupka, A.; Malmsten, M. *J. Biol. Chem.* **2009**, *284* (26), 17584–17594.
(34) Sonesson, A.; Nordahl, E. A.; Malmsten, M.; Schmidtchen, A. *Int. J. Pept.* **2011**, *2011*, 761037, 1–11.
(35) Malmsten, M.; Kasetty, G.; Pasupuleti, M.; Alenfall, J.; Schmidtchen, A. *PLoS One* **2011**, *6* (1), e16400.
(36) Eckert, R. *Future Microbiol.* **2011**, *6* (6), 635–651.
(37) Kalle, M.; Papareddy, P.; Kasetty, G.; van der Plas, M. J. A.; Mörgelin, M.; Malmsten, M.; Schmidtchen, A. *PLoS One* **2014**, *9* (7), e102577.
(38) Singh, S.; Papareddy, P.; Mörgelin, M.; Schmidtchen, A.; Malmsten, M. *Biomacromolecules* **2014**, *15* (4), 1337–1345.
(39) Ilyas, H.; Kim, J.; Lee, D.; Malmsten, M.; Bhunia, A. *J. Biol. Chem.* **2019**, *294* (40), 14615–14633.
(40) Kalle, M.; Papareddy, P.; Kasetty, G.; Tollefsen, D. M.; Malmsten, M.; Mörgelin, M.; Schmidtchen, A. *J. Immunol.* **2013**, *190* (12), 6303–6310.
(41) Nyström, L.; Strömstedt, A. A.; Schmidtchen, A.; Malmsten, M. *Biomacromolecules* **2018**, *19* (8), 3456–3466.
(42) Malmsten, M.; Emoto, K.; Van Alstine, J. M. *J. Colloid Interface Sci.* **1998**, *202* (2), 507–517.
(43) Gref, R.; Minamitake, Y.; Peracchia, M.; Trubetskoy, V.; Torchilin, V.; Langer, R. *Science.* **1994**, *263* (5153), 1600–1603.
(44) Veronese, F. M.; Mero, A. *BioDrugs* **2008**, *22* (5), 315–329.
(45) Dürr, U. H. N.; Sudheendra, U. S.; Ramamoorthy, A. *Biochimica et Biophysica Acta - Biomembranes*. **2006**, *1758* (9), 1408–1425.

(46) Reinholz, M.; Ruzicka, T.; Schauber, J. *Ann. Dermatol.* **2012**, *24* (2), 126–135.
(47) Bittencourt, C. R.; De Oliveira Farias, E. A.; Bezerra, K. C.; Véras, L. M. C.; Silva, V. C.; Costa, C. H. N.; Bemquerer, M. P.; Silva, L. P.; Souza De Almeida Leite, J. R. De; Eiras, C. *Mater. Sci. Eng. C* **2016**, *59*, 549–555.
(48) Shahmiri, M.; Enciso, M.; Adda, C. G.; Smith, B. J.; Perugini, M. A.; Mechler, A. *Sci. Rep.* **2016**, *6* (1), 38184.
(49) Henzler Wildman, K. A.; Lee, D. K.; Ramamoorthy, A. *Biochemistry* **2003**, *42* (21), 6545–6558.
(50) Nordström, R.; Nyström, L.; Andrén, O. C. J.; Malkoch, M.; Umerska, A.; Davoudi, M.; Schmidtchen, A.; Malmsten, M. *J. Colloid Interface Sci.* **2018**, *513*, 141–150.
(51) Turner, J.; Cho, Y.; Dinh, N.-N.; Alan, J.; Lehrer, R. I.; Waring, A. J. **1998**, *42* (9), 2206–2214.
(52) Thwaite, J. E.; Hibbs, S.; Titball, R. W.; Atkins, T. P. *Antimicrob. Agents Chemother.* **2006**, *50* (7), 2316–2322.
(53) Sivertsen, A.; Isaksson, J.; Leiros, H.-K. S.; Svenson, J.; Svendsen, J.-S.; Brandsdal, B. O. *BMC Struct. Biol.* **2014**, *14* (1), 4.
(54) Svenson, J.; Brandsdal, B. O.; Stensen, W.; Svendsen, J. S. *J. Med. Chem.* **2007**, *50* (14), 3334–3339.
(55) Kapoor, R.; Eimerman, P. R.; Hardy, J. W.; Cirillo, J. D.; Contag, C. H.; Barron, A. E. *Antimicrob. Agents Chemother.* **2011**, *55* (6), 3058–3062.
(56) Queval, C. J.; Brosch, R.; Simeone, R. *Front. Microbiol.* **2017**, *8*, 2284.
(57) VanderVen, B. C.; Fahey, R. J.; Lee, W.; Liu, Y.; Abramovitch, R. B.; Memmott, C.; Crowe, A. M.; Eltis, L. D.; Perola, E.; Deininger, D. D.; Wang, T.; Locher, C. P.; Russell, D. G. *PLoS Pathog.* **2015**, *11* (2), e1004679.
(58) Moncla, B. J.; Pryke, K.; Rohan, L. C.; Graebing, P. W. *Adv. Biosci. Biotechnol.* **2011**, *2* (6), 404–408.
(59) Nordström, R.; Malmsten, M. *Adv. Colloid Interface Sci.* **2017**, *242*, 17–34.
(60) Biswaro, L. S.; da Costa Sousa, M. G.; Rezende, T. M. B.; Dias, S. C.; Franco, O. L. *Front. Microbiol.* **2018**, *9*, 855.
(61) Sobczak, M.; Dębek, C.; Olędzka, E.; Kozłowski, R. *Molecules* **2013**, *18* (11), 14122–14137.
(62) Zetterberg, M. M.; Reijmar, K.; Pränting, M.; Engström, Å.; Andersson, D. I.; Edwards, K. *J. Control. Release* **2011**, *156* (3), 323–328.
(63) Malekkhaiat Häffner, S.; Nyström, L.; Nordström, R.; Xu, Z. P.; Davoudi, M.; Schmidtchen, A.; Malmsten, M. *Phys. Chem. Chem. Phys.* **2017**, *19* (35), 23832–23842.
(64) Tenland, E.; Pochert, A.; Krishnan, N.; Umashankar Rao, K.; Kalsum, S.; Braun, K.; Glegola-Madejska, I.; Lerm, M.; Robertson, B. D.; Lindén, M.; Godaly, G. *PLoS One* **2019**, *14* (2), e0212858.
(65) Carmona-Ribeiro, A. M.; de Melo Carrasco, L. D. *Int. J. Mol. Sci.* **2014**, *15* (10), 18040–18083.
(66) Malmsten, M.; Bysell, H.; Hansson, P. *Curr. Opin. Colloid Interface Sci.* **2010**, *15* (6), 435–444.
(67) Bray, B. L. *Nat. Rev. Drug Discov.* **2003**, *2* (7), 587–593.
(68) Braun, K.; Pochert, A.; Lindén, M.; Davoudi, M.; Schmidtchen, A.; Nordström, R.; Malmsten, M. *J. Colloid Interface Sci.* **2016**, *475*, 161–170.
(69) Izquierdo-Barba, I.; Vallet-Regí, M.; Kupferschmidt, N.; Terasaki, O.; Schmidtchen, A.; Malmsten, M. *Biomaterials* **2009**, *30* (29), 5729–5736.
(70) Dong, A.; Zhang, Q.; Wang, T.; Wang, W.; Liu, F.; Gao, G. *J. Phys. Chem. C* **2010**, *114* (41), 17298–17303.

(71) Chen, W.-Y.; Chang, H.-T. H.-Y.; Lu, J.-K.; Huang, Y.-C.; Harroun, S. G.; Tseng, Y.-T.; Li, Y.-J.; Huang, C.-C.; Chang, H.-T. H.-Y. *Adv. Funct. Mater.* **2015**, *25* (46), 7189–7199.
(72) Lambadi, P. R.; Sharma, T. K.; Kumar, P.; Vasnani, P.; Thalluri, S. M.; Bisht, N.; Pathania, R.; Navani, N. K. *Int. J. Nanomedicine* **2015**, *10*, 2155–2171.
(73) Kanchanapally, R.; Viraka Nellore, B. P.; Sinha, S. S.; Pedraza, F.; Jones, S. J.; Pramanik, A.; Chavva, S. R.; Tchounwou, C.; Shi, Y.; Vangara, A.; Sardar, D.; Ray, P. C. *RSC Adv.* **2015**, *5* (24), 18881–18887.
(74) Shim, G.; Lee, J.; Kim, J.; Lee, H.-J.; Kim, Y. B.; Oh, Y.-K. *RSC Adv.* **2015**, *5* (62), 49905–49913.
(75) Boge, L.; Bysell, H.; Ringstad, L.; Wennman, D.; Umerska, A.; Cassisa, V.; Eriksson, J.; Joly-Guillou, M. L.; Edwards, K.; Andersson, M. *Langmuir* **2016**, *32* (17), 4217–4228.
(76) Taylor, T. M.; Gaysinsky, S.; Davidson, P. M.; Bruce, B. D.; Weiss, J. *Food Biophys.* **2007**, *2* (1), 1–9.
(77) Mizukami, S.; Kashibe, M.; Matsumoto, K.; Hori, Y.; Kikuchi, K. *Chem. Sci.* **2017**, *8* (4), 3047–3053.
(78) Sebe, I.; Ostorhazi, E.; Fekete, A.; Kovacs, K. N.; Zelko, R.; Kovalszky, I.; Li, W.; Wade, J. D.; Szabo, D.; Otvos, L. *Amino Acids* **2016**, *48* (1), 203–211.
(79) Shukla, A.; Fleming, K. E.; Chuang, H. F.; Chau, T. M.; Loose, C. R.; Stephanopoulos, G. N.; Hammond, P. T. *Biomaterials* **2010**, *31* (8), 2348–2357.
(80) Shi, J.; Liu, Y.; Wang, Y.; Zhang, J.; Zhao, S.; Yang, G. *Sci. Rep.* **2015**, *5*, 16336.
(81) Water, J. J.; Kim, Y.; Maltesen, M. J.; Franzyk, H.; Foged, C.; Nielsen, H. M. *Pharm. Res.* **2015**, *32* (8), 2727–2735.
(82) Silva, J. P.; Gonçalves, C.; Costa, C.; Sousa, J.; Silva-Gomes, R.; Castro, A. G.; Pedrosa, J.; Appelberg, R.; Gama, F. M. *J. Control. Release* **2016**, *235*, 112–124.
(83) Singh, S.; Datta, A.; Borro, B. C.; Davoudi, M.; Schmidtchen, A.; Bhunia, A.; Malmsten, M. *ACS Appl. Mater. Interfaces* **2017**, *9* (46), 40094–40106.
(84) Wu, C.; Wu, T.; Fang, Z.; Zheng, J.; Xu, S.; Chen, S.; Hu, Y.; Ye, X. *RSC Adv.* **2016**, *6* (52), 46686–46695.
(85) Yüksel, E.; Karakeçili, A.; Demirtaş, T. T.; Gümüşderelioğlu, M. *Int. J. Biol. Macromol.* **2016**, *86*, 162–168.
(86) Cruz, J.; Flórez, J.; Torres, R.; Urquiza, M.; Gutiérrez, J. A.; Guzmán, F.; Ortiz, C. C. *Nanotechnology* **2017**, *28* (13), 135102.
(87) Etienne, O.; Picart, C.; Taddei, C.; Haikel, Y.; Dimarcq, J. L.; Schaaf, P.; Voegel, J. C.; Ogier, J. A.; Egles, C. *Antimicrob. Agents Chemother.* **2004**, *48* (10), 3662–3669.
(88) Bysell, H.; Månsson, R.; Hansson, P.; Malmsten, M. *Adv. Drug Deliv. Rev.* **2011**, *63* (13), 1172–1185.
(89) Frokjaer, S.; Otzen, D. E. *Nat. Rev. Drug Discov.* **2005**, *4* (4), 298–306.
(90) Rodriguez, B. E.; Wolfe, M. S.; Fryd, M. *Macromolecules* **1994**, *27* (22), 6642–6647.
(91) Dalmont, H., Pinprayoon, O., Saunders, B. R. *Langmuir* **2008**, *24* (6), 2834-2840.
(92) Tam, K. C.; Ragaram, S.; Pelton, R. H. *Langmuir* **1994**, *10* (2), 418–422.
(93) Pelton, R. *Adv. Colloid Interface Sci.* **2000**, *85* (1), 1–33.
(94) Nolan, C. M.; Gelbaum, L. T.; Lyon, L. A.; Christine M. Nolan; Leslie T. Gelbaum; Lyon, L. A. *Biomacromolecules* **2006**, *7* (10), 2918–2922.

(95) Li, H.; Voci, S.; Ravaine, V.; Sojic, N. *J. Phys. Chem. Lett.* **2018**, *9* (2), 340–345.
(96) Liu, Y.; Tsao, C.-Y.; Kim, E.; Tschirhart, T.; Terrell, J. L.; Bentley, W. E.; Payne, G. F. *Adv. Healthc. Mater.* **2017**, *6* (1), 1600908.
(97) Park, J.; Pramanick, S.; Park, D.; Yeo, J.; Lee, J.; Lee, H.; Kim, W. J. *Adv. Mater.* **2017**, *29* (44), 1702859.
(98) Gu, Z.; Dang, T. T.; Ma, M.; Tang, B. C.; Cheng, H.; Jiang, S.; Dong, Y.; Zhang, Y.; Anderson, D. G. *ACS Nano* **2013**, *7* (8), 6758–6766.
(99) Sung, B.; Shaffer, S.; Sittek, M.; Alboslemy, T.; Kim, C.; Kim, M.-H. *J. Vis. Exp.* **2016**, 108, 53680.
(100) Dong, H.; Mantha, V.; Matyjaszewski, K. *Chem. Mater.* **2009**, *21* (17), 3965–3972.
(101) Klinger, D.; Landfester, K. *Soft Matter* **2011**, *7* (4), 1426–1440.
(102) Nyström, L.; Nordström, R.; Bramhill, J.; Saunders, B. R.; Álvarez-Asencio, R.; Rutland, M. W.; Malmsten, M. *Biomacromolecules* **2016**, *17* (2), 669–678.
(103) Cleophas, R. T. C.; Riool, M.; Quarles van Ufford, H. (Linda) C.; Zaat, S. A. J.; Kruijtzer, J. A. W.; Liskamp, R. M. J. *ACS Macro Lett.* **2014**, *3* (5), 477–480.
(104) Sun, Y.; Liu, Y.; Liu, W.; Lu, C.; Wang, L. *Biochem. Eng. J.* **2015**, *95*, 78–85.
(105) Zhou, C.; Li, P.; Qi, X.; Sharif, A. R. M.; Poon, Y. F.; Cao, Y.; Chang, M. W.; Leong, S. S. J.; Chan-Park, M. B. *Biomaterials* **2011**, *32* (11), 2704–2712.
(106) Cleophas, R. T. C.; Sjollema, J.; Busscher, H. J.; Kruijtzer, J. A. W.; Liskamp, R. M. J. *Biomacromolecules* **2014**, *15* (9), 3390–3395.
(107) Nordström, R.; Andrén, O. C. J.; Singh, S.; Malkoch, M.; Davoudi, M.; Schmidtchen, A.; Malmsten, M. *J. Colloid Interface Sci.* **2019**, *554*, 592–602.
(108) Zhang, Y.; Andrén, O. C. J.; Nordström, R.; Fan, Y.; Malmsten, M.; Mongkhontreerat, S.; Malkoch, M. *Adv. Funct. Mater.* **2019**, 1806693.
(109) Bysell, H.; Hansson, P.; Malmsten, M. *J. Phys. Chem. B* **2010**, *114* (21), 7207–7215.
(110) Månsson, R.; Frenning, G.; Malmsten, M. *Biomacromolecules* **2013**, *14* (7), 2317–2325.
(111) Bysell, H.; Malmsten, M. *Langmuir* **2006**, *22* (12), 5476–5484.
(112) Bysell, H.; Schmidtchen, A.; Malmsten, M. *Biomacromolecules* **2009**, *10* (8), 2162–2168.
(113) Bysell, H.; Malmsten, M. *Langmuir* **2008**, *25* (1), 522–528.
(114) Bysell, H.; Hansson, P.; Schmidtchen, A.; Malmsten, M. *J. Phys. Chem. B* **2010**, *114* (3), 1307–1313.
(115) Månsson, R.; Bysell, H.; Hansson, P.; Schmidtchen, A.; Malmsten, M. *Biomacromolecules* **2011**, *12* (2), 419–424.
(116) Bysell, H.; Månsson, R.; Malmsten, M.; Mansson, R.; Malmsten, M. *Colloids Surf., A* **2011**, *391* (1–3), 62–68.
(117) Zelezetsky, I.; Pontillo, A.; Puzzi, L.; Antcheva, N.; Segat, L.; Pacor, S.; Crovella, S.; Tossi, A. *J. Biol. Chem.* **2006**, *281* (29), 19861–19871.
(118) Morgera, F.; Vaccari, L.; Antcheva, N.; Scaini, D.; Pacor, S.; Tossi, A. *Biochem. J.* **2009**, *417* (3), 727–735.
(119) Patra, J. K.; Das, G.; Fraceto, L. F.; Campos, E. V. R.; Rodriguez-Torres, M. D. P.; Acosta-Torres, L. S.; Diaz-Torres, L. A.; Grillo, R.; Swamy, M. K.; Sharma, S.; Habtemariam, S.; Shin, H.-S. *J. Nanobiotechnology* **2018**, *16*, 71.
(120) Fleige, E.; Quadir, M. A.; Haag, R. *Adv. Drug Deliv. Rev.* **2012**, *64* (9), 866–884.
(121) Andrén, Oliver. C. J. Malkoch, M.; Zhang, Y.; Nordström, R. Dendritic nanogel carriers and method of production. 1850975–2, **2018**.

(122) Lally, S.; Mackenzie, P.; LeMaitre, C. L.; Freemont, T. J.; Saunders, B. R. *J. Colloid Interface Sci.* **2007**, *316* (2), 367–375.
(123) Li, J.; Mooney, D. J. *Nat. Rev. Mater.* **2016**, *1* (12), 16071.
(124) Wistrand-Yuen, E.; Knopp, M.; Hjort, K.; Koskiniemi, S.; Berg, O. G.; Andersson, D. I. *Nat. Commun.* **2018**, *9* (1), 1599.
(125) Zhang, Y.; Chan, H. F.; Leong, K. W. *Adv. Drug Deliv. Rev.* **2013**, *65* (1), 104–120.
(126) Fu, Y.; Kao, W. J. *Expert Opin. Drug Deliv.* **2010**, *7* (4), 429–444.
(127) Kamath, K. R.; Park, K. *Adv. Drug Deliv. Rev.* **1993**, *11*, 59–84.
(128) Nair, L. S.; Laurencin, C. T. *Prog. Polym. Sci.* **2007**, *32* (8–9), 762–798.
(129) Owens, D. E.; Peppas, N. A. *Int. J. Pharm.* **2006**, *307* (1), 93–102.
(130) He, Q.; Zhang, J.; Shi, J.; Zhu, Z.; Zhang, L.; Bu, W.; Guo, L.; Chen, Y. *Biomaterials* **2010**, *31* (6), 1085–1092.
(131) Veronese, F. M.; Pasut, G. *Drug Discov. Today* **2005**, *10* (21), 1451–1458.
(132) Henry, C. E.; Wang, Y.-Y.; Yang, Q.; Hoang, T.; Chattopadhyay, S.; Hoen, T.; Ensign, L. M.; Nunn, K. L.; Schroeder, H.; McCallen, J.; Moench, T.; Cone, R.; Roffler, S. R.; Lai, S. K. *Acta Biomater.* **2016**, *43*, 61–70.
(133) Grenier, P.; Viana, I. M. de O.; Lima, E. M.; Bertrand, N. *J. Control. Release* **2018**, *287*, 121–131.
(134) Lubich, C.; Allacher, P.; de la Rosa, M.; Bauer, A.; Prenninger, T.; Horling, F. M.; Siekmann, J.; Oldenburg, J.; Scheiflinger, F.; Reipert, B. M. *Pharm. Res.* **2016**, *33* (9), 2239–2249.
(135) Maier, K. E.; Rusconi, C. P.; Levy, M. *Cell Chem. Biol.* **2019**, *26* (5), 615–616.
(136) Xue, W.; Liu, Y.; Zhang, N.; Yao, Y.; Ma, P.; Wen, H.; Huang, S.; Luo, Y. E.; Fan, H. *Int. J. Nanomedicine* **2018**, *Volume 13*, 5719–5731.
(137) Hollmann, A.; Martinez, M.; Maturana, P.; Semorile, L. C.; Maffia, P. C. *Front. Chem.* **2018**, *6*, 204.
(138) Sohlenkamp, C.; Geiger, O. *FEMS Microbiol. Rev.* **2016**, *40* (1), 133–159.
(139) Epand, R. F.; Savage, P. B.; Epand, R. M. *Biochim. Biophys. Acta - Biomembr.* **2007**, *1768* (10), 2500–2509.
(140) van Meer, G. *Annu. Rev. Cell Biol.* **1989**, *5* (1), 247–275.
(141) Reichmann, N. T.; Gründling, A. *FEMS Microbiol. Lett.* **2011**, *319* (2), 97–105.
(142) Raetz, C. R. H.; Dowhan, W. *Journal of Biological Chemistry*. **1990**, 1235–1238.
(143) Fensterseifer, I. C. M.; Felício, M. R.; Alves, E. S. F.; Cardoso, M. H.; Torres, M. D. T.; Matos, C. O.; Silva, O. N.; Lu, T. K.; Freire, M. V.; Neves, N. C.; Gonçalves, S.; Lião, L. M.; Santos, N. C.; Porto, W. F.; de la Fuente-Nunez, C.; Franco, O. L. *Biochim. Biophys. Acta - Biomembr.* **2019**, *1861* (7), 1375–1387.
(144) Volzing, K.; Borrero, J.; Sadowsky, M. J.; Kaznessis, Y. N. *ACS Synth. Biol.* **2013**, *2* (11), 643–650.
(145) Li, J.; Koh, J.-J.; Liu, S.; Lakshminarayanan, R.; Verma, C. S.; Beuerman, R. W. *Front. Neurosci.* **2017**, *11*, 73
(146) Alberts, B.; Johnson, A.; Lewis, J.; Morgan, D. *Molecular biology of the cell*; Garland Science, **2015**.
(147) Paulson, J. C. *Trends Biochem. Sci.* **1989**, *14* (7), 272–276.
(148) Strömstedt, A. A. A.; Ringstad, L.; Schmidtchen, A.; Malmsten, M. *Curr. Opin. Colloid Interface Sci.* **2010**, *15* (6), 467–478.
(149) Ringstad, L.; Schmidtchen, A.; Malmsten, M. *Langmuir* **2006**, *22* (11), 5042–5050.

(150) Singh, S.; Kasetty, G.; Schmidtchen, A.; Malmsten, M. *Biochim. Biophys. Acta - Biomembr.* **2012**, *1818* (9), 2244–2251.
(151) Marr, A. G.; Ingraham, J. L. *J. Bacteriol.* **1962**, *84* (6), 1260–1267.
(152) Buehler, L. K. *Cell membranes*, 1st ed.; Garland Science: London, **2015**.
(153) Cevc, G. *Phospholipids handbook*, 1st ed.; Cevc, G., Ed.; Marcel Dekker: New York, **1993**.
(154) Yeagle, P. *The membranes of cells*, 3rd ed.; Academic press Inc.: San Diego, **2016**.
(155) van Meer, G.; de Kroon, A. I. P. M. *J. Cell Sci.* **2011**, *124* (Pt 1), 5–8.
(156) Strömstedt, A. A.; Wessman, P.; Ringstad, L.; Edwards, K.; Malmsten, M. *J. Colloid Interface Sci.* **2007**, *311* (1), 59–69.
(157) Lally, S.; Liu, R.; Supasuteekul, C.; Saunders, B. R.; Freemont, T. *J. Mater. Chem.* **2011**, *21* (44), 17719.
(158) Nishida, S.; El-Aasser, M. S.; Klein, A.; Vanderhoff, J. W. In *Emulsion Polymers and Emulsion Polymerization*; American Chemical Society, **2009**; 291–314.
(159) Almgren, M.; Edwards, K.; Karlsson, G. *Colloids Surfaces A Physicochem. Eng. Asp.* **2000**, *174* (1–2), 3–21.
(160) Kuntsche, J.; Horst, J. C.; Bunjes, H. *Int. J. Pharm.* **2011**, *417* (1–2), 120–137.
(161) Goldstein, J. I.; Newbury, D. E.; Echlin, P.; Joy, D. C.; Lyman, C. E.; Lifshin, E.; Sawyer, L.; Michael, J. R. *Scanning Electron Microscopy and X-ray Microanalysis*, 3rd ed.; Springer US: Boston, MA, **2003**.
(162) Garcia-Salinas, M. J.; Donald, A. M. *J. Colloid Interface Sci.* **2010**, *342* (2), 629–635.
(163) Donald, A. M. *Nat. Mater.* **2003**, *2* (8), 511–516.
(164) Wiedemair, J.; Serpe, M. J.; Kim, J.; Masson, J. F.; Lyon, L. A.; Mizaikoff, B.; Kranz, C. *Langmuir* **2007**, *23* (1), 130–137.
(165) Foster, B. *Am. Lab.* **2012**, *44* (4), 24–27.
(166) Rowe, M. D.; Eyiler, E.; Walters, K. B. *Polym. Test.* **2016**, *52*, 192–199.
(167) Goldburg, W. I. *Am. J. Phys.* **1999**, *67* (12), 1152–1160.
(168) Bhattacharjee, S. *J. Control. Release* **2016**, *235*, 337–351.
(169) Dragovic, R. A.; Gardiner, C.; Brooks, A. S.; Tannetta, D. S.; Ferguson, D. J. P.; Hole, P.; Carr, B.; Redman, C. W. G.; Harris, A. L.; Dobson, P. J.; Harrison, P.; Sargent, I. L. *Nanomedicine Nanotechnology, Biol. Med.* **2011**, *7* (6), 780–788.
(170) Filipe, V.; Hawe, A.; Jiskoot, W. *Pharm. Res.* **2010**, *27* (5), 796–810.
(171) Larryisgood. Zeta Potential commons.wikimedia.org (accessed Aug 20, 2019).
(172) Joseph, E.; Singhvi, G. *Multifunctional nanocrystals for cancer therapy: a potential nanocarrier*; William Andrew Publishing, **2019**.
(173) Delgado, A. V.; González-Caballero, F.; Hunter, R. J.; Koopal, L. K.; Lyklema, J. *J. Colloid Interface Sci.* **2007**, *309* (2), 194–224.
(174) Stieger, M.; Richtering, W.; Pedersen, J. S.; Lindner, P. *J. Chem. Phys.* **2004**, *120* (13), 6197–6206.
(175) Wong, A. K. Y.; Krull, U. J. *Anal. Bioanal. Chem.* **2005**, *383* (2), 187–200.
(176) Alvarez-Román, R.; Naik, A.; Kalia, Y. .; Fessi, H.; Guy, R. . *Eur. J. Pharm. Biopharm.* **2004**, *58* (2), 301–316.
(177) Schneider, C. A.; Rasband, W. S.; Eliceiri, K. W. *Nat. Methods* **2012**, *9* (7), 671–675.
(178) Vacklin, H. P.; Tiberg, F.; Fragneto, G.; Thomas, R. K. *Biochemistry* **2005**, *44* (8), 2811–2821.
(179) Tiberg, F.; Harwigsson, I.; Malmsten, M. *Eur. Biophys. J.* **2000**, *29* (3), 196–203.

(180) Smith, P. K.; Krohn, R. I.; Hermanson, G. T.; Mallia, A. K.; Gartner, F. H.; Provenzano, M. D.; Fujimoto, E. K.; Goeke, N. M.; Olson, B. J.; Klenk, D. C. *Anal. Biochem.* **1985**, *150* (1), 76–85.
(181) Bakshi, K.; Liyanage, M. R.; Volkin, D. B.; Middaugh, C. R. In *Therapeutic Peptides, Methods and Protocols*; Andrew E. Nixon, Ed.; Humana Press: Totowa, NJ, **2014**; 247–253.
(182) Greenfield, N. J.; Fasman, G. D. *Biochemistry* **1969**, *8* (10), 4108–4116.
(183) Sjögren, H.; Ulvenlund, S. *Biophys. Chem.* **2005**, *116* (1), 11–21.
(184) Whitmore, L.; Wallace, B. A. *Biopolymers* **2008**, *89* (5), 392–400.
(185) Miles, A. J.; Wallace, B. A. *Chem. Soc. Rev.* **2016**, *45* (18), 4859–4872.
(186) Güntert, P. In *Protein NMR Techniques. Methods in Molecular Biology*; Downing, A. K., Ed.; Humana Press: New Jersey, **2004**; 353–378.
(187) The PyMOL Molecular Graphics System. Schrödinger LCC **2002**.
(188) Koradi, R.; Billeter, M.; Wüthrich, K. *J. Mol. Graph.* **1996**, *14* (1), 51–55.
(189) Pettersen, E. F.; Goddard, T. D.; Huang, C. C.; Couch, G. S.; Greenblatt, D. M.; Meng, E. C.; Ferrin, T. E. *J. Comput. Chem.* **2004**, *25* (13), 1605–1612.
(190) Bhunia, A.; Bhattacharjya, S.; Chatterjee, S. *Drug Discov. Today* **2012**, *17* (9–10), 505–513.
(191) Stott, K.; Stonehouse, J.; Keeler, J.; Hwang, T.-L.; Shaka, A. J. *J. Am. Chem. Soc.* **1995**, *117* (14), 4199–4200.
(192) Mayer, M.; Meyer, B. *J. Am. Chem. Soc.* **2001**, *123* (25), 6108–6117.
(193) Weinstein, J. N.; Blumenthal, R.; Klausner, R. D. *Methods Enzymol.* **1986**, *128*, 657–668.
(194) Ringstad, L.; Andersson Nordahl, E.; Schmidtchen, A.; Malmsten, M. *Biophys. J.* **2007**, *92* (1), 87–98.
(195) Singh, S.; Kalle, M.; Papareddy, P.; Schmidtchen, A.; Malmsten, M. *Biomacromolecules* **2013**, *14* (5), 1482–1492.
(196) Jiang, M.; Popa, I.; Maroni, P.; Borkovec, M. *Colloids Surfaces A Physicochem. Eng. Asp.* **2010**, *360* (1–3), 20–25.
(197) Ringstad, L. *Interaction Between Antimicrobial Peptides and Phospholipid Membranes: Effects of Peptide Length and Composition*; Acta Universitatis Upsaliensis: Uppsala, **2009**.
(198) Csúcs, G.; Ramsden, J. J. *Biochim. Biophys. Acta - Biomembr.* **1998**, *1369* (1), 61–70.
(199) Halthur, T. J.; Elofsson, U. M. *Langmuir* **2004**, *20* (5), 1739–1745.
(200) Kalb, E.; Frey, S.; Tamm, L. K. *Biochim. Biophys. Acta - Biomembr.* **1992**, *1103* (2), 307–316.
(201) Fragneto-Cusani, G. *J. Phys. Condens. Matter* **2001**, *13* (21), 4973–4989.
(202) Fernandez, D. I.; Le Brun, A. P.; Whitwell, T. C.; Sani, M.-A.; James, M.; Separovic, F. *Phys. Chem. Chem. Phys.* **2012**, *14* (45), 15739.
(203) Zhou, X.-L.; Chen, S.-H. *Phys. Rep.* **1995**, *257* (4–5), 223–348.
(204) Squires, G. L. *Introduction to the Theory of Thermal Neutron Scattering*; Cambridge University Press: Cambridge, **2012**.
(205) Cappelletti, R. L.; Glinka, C. J.; Krueger, S.; Lindstrom, R. A.; Lynn, J. W.; Prask, H. J.; Prince, E.; Rush, J. J.; Rowe, J. M.; Satija, S. K.; Toby, B. H.; Tsai, A.; Udovic, T. J. *J. Res. Natl. Inst. Stand. Technol.* **2001**, *106* (1), 187–230.
(206) Cubitt, R.; Fragneto, G. *Scattering* **2002**, 1198–1208.
(207) Wacklin, H. P. *Curr. Opin. Colloid Interface Sci.* **2010**, *15* (6), 445–454.
(208) Krueger, S. *Curr. Opin. Colloid Interface Sci.* **2001**, *6* (2), 111–117.
(209) Majkrzak, C. F.; Carpenter, E.; Heinrich, F.; Berk, N. F. *J. Appl. Phys.* **2011**, *110* (10), 102212.

(210) Boge, L.; Browning, K. L.; Nordstrom, R.; Campana, M.; Damgaard, L. S. E.; Seth Caous, J.; Hellsing, M. S.; Ringstad, L.; Anderssson, M. *ACS Appl. Mater. Interfaces* **2019**, *11* (24), 21314–21322.
(211) Hughes, A. *RasCAL*; **2014**.
(212) Shai, Y. *Biochim. Biophys. Acta - Biomembr.* **2013**, *1828* (10), 2306–2313.
(213) Tatulian, S. A. In *Methods in Enzymology*; Gelb, M. H., Ed.; Elsevier, **2017**; Vol. 583, 197–230.
(214) Lacey A. Averett; Griffiths, P. R.; Nishikida, K. *Anal. Chem.* **2008**, *80* (8), 3045–3049.
(215) Chen, X.; Wang, J.; Boughton, A. P.; Kristalyn, C. B.; Chen, Z. *J. Am. Chem. Soc.* **2007**, *129* (5), 1420–1427.
(216) Nguyen, K. T.; Le Clair, S. V.; Ye, S.; Chen, Z. *J. Phys. Chem. B* **2009**, *113* (36), 12358–12363.
(217) Andrews, J. M. *J. Antimicrob. Chemother.* **2001**, *48* (suppl_1), 5–16.
(218) Stromstedt, A. A.; Pasupuleti, M.; Schmidtchen, A.; Malmsten, M. *Antimicrob. Agents Chemother.* **2009**, *53* (2), 593–602.
(219) Starr, C. G.; Wimley, W. C. *Biochim. Biophys. Acta - Biomembr.* **2017**, *1859* (12), 2319–2326.
(220) Borukhov, I.; Andelman, D.; Borrega, R.; Cloitre, M.; Leibler, L.; Orland, H. *J. Phys. Chem. B* **2000**, *104* (47), 11027–11034.
(221) Sawant, K. K.; Dodiya, S. S. *Recent Pat. Drug Deliv. Formul.* **2008**, *2* (2), 120–135.
(222) Nordström, R.; Nyström, L.; Ilyas, H.; Atreya, H. S.; Borro, B. C.; Bhunia, A.; Malmsten, M. *Colloids Surfaces A Physicochem. Eng. Asp.* **2019**, *565*, 8–15.
(223) Porcelli, F.; Verardi, R.; Shi, L.; Henzler-Wildman, K. A.; Ramamoorthy, A.; Veglia, G. *Biochemistry* **2008**, *47* (20), 5565.
(224) Lee, C.-C.; Sun, Y.; Qian, S.; Huang, H. W. *Biophys. J.* **2011**, *100* (7), 1688–1696.
(225) Vitiello, G.; Falanga, A.; Galdiero, M.; Marsh, D.; Galdiero, S.; D'Errico, G. *Biochim. Biophys. Acta - Biomembr.* **2011**, *1808* (10), 2517–2526.
(226) Sevcsik, E.; Pabst, G.; Richter, W.; Danner, S.; Amenitsch, H.; Lohner, K. *Biophys. J.* **2008**, *94* (12), 4688–4699.
(227) Henzler-Wildman, K. A.; Martinez, G. V.; Brown, M. F.; Ramamoorthy, A. *Biochemistry* **2004**, *43* (26), 8459–8469.
(228) Margitta, D.; Michael, S.; Torsten, W.; Anett, W.; Michael, B.; Eberhard, K.; Katsumi, M.; Osamu, M.; Bienert, M. *Biochemistry* **1996**, *35* (38), 12612–12622.
(229) Kim, H.; Jang, J. H.; Kim, S. C.; Cho, J. H. *J. Antimicrob. Chemother.* **2014**, *69* (1), 121–132.

Acta Universitatis Upsaliensis

Digital Comprehensive Summaries of Uppsala Dissertations from the Faculty of Pharmacy 280

Editor: The Dean of the Faculty of Pharmacy

A doctoral dissertation from the Faculty of Pharmacy, Uppsala University, is usually a summary of a number of papers. A few copies of the complete dissertation are kept at major Swedish research libraries, while the summary alone is distributed internationally through the series Digital Comprehensive Summaries of Uppsala Dissertations from the Faculty of Pharmacy. (Prior to January, 2005, the series was published under the title "Comprehensive Summaries of Uppsala Dissertations from the Faculty of Pharmacy".)

Distribution: publications.uu.se
urn:nbn:se:uu:diva-383639

ACTA
UNIVERSITATIS
UPSALIENSIS
UPPSALA
2019